Published in final edited form as:
Nature. 2014 March 27; 507(7493): 508–512. doi:10.1038/nature12998.

The E3 Ligase Cbl-b and TAM receptors regulate cancer metastasis via natural killer cells

Magdalena Paolino[1], **Axel Choidas**[2], **Stephanie Wallner**[3], **Blanka Pranjic**[1], **Iris Uribesalgo**[1], **Stefanie Loeser**[1], **Amanda M. Jamieson**[4], **Wallace Y. Langdon**[5], **Fumiyo Ikeda**[1], **Juan P. Fededa**[1], **Shane J. Cronin**[1], **Roberto Nitsch**[1], **Carsten Schultz-Fademrecht**[2], **Jan Eickhoff**[2], **Sascha Menninger**[2], **Anke Unger**[2], **Robert Torka**[6], **Thomas Gruber**[3], **Reinhard Hinterleitner**[3], **Gottfried Baier**[3], **Dominik Wolf**[3,7], **Axel Ullrich**[6], **Bert M. Klebl**[2], and **Josef M. Penninger**[1]

[1]IMBA, Institute of Molecular Biotechnology of the Austrian Academy of Sciences, 1030 Vienna, Austria

[2]Lead Discovery Center GmbH, D-44227 Dortmund, Germany

[3]Medical University Innsbruck, 6020 Innsbruck, Austria

[4]Max F. Perutz Laboratories, University of Vienna, 1030 Vienna, Austria

[5]School of Pathology and Laboratory Medicine, University of Western Australia, Crawley WA 6009, Perth, Australia

[6]Max-Planck Institute for Biochemistry, Department of Molecular Biology, D-82152 Martinsried, Germany

[7]Internal Medicine III, University Hospital Bonn, 53127 Bonn, Germany

Summary

Tumor metastasis is the primary cause of mortality in cancer patients and remains the major challenge for cancer therapy1. New therapeutic approaches to block inhibitory pathways of the immune system have renewed hopes for the utility of such therapies2. Here we show that genetic deletion of the E3 ubiquitin ligase Cbl-b (Casitas B cell lymphoma-b) or targeted inactivation of its E3 ligase activity licenses natural killer (NK) cells to spontaneously reject metastatic tumors. The TAM tyrosine kinase receptors Tyro3, Axl, and Mer were identified as ubiquitylation

Correspondence and requests for materials should be addressed to Josef M. Penninger, IMBA, Dr. Bohr Gasse 3, A-1030 Vienna. Tel. 43-1-79044 ext 4702; Fax 43-1-79044 4701, josef.penninger@imba.oeaw.ac.at.

Author contributions. All experiments, with the exceptions listed below, were performed by M.P. B.P. helped with mouse dissections, *in vivo* administration of LDC1267 and melanoma lung tumors quantifications. I.U. helped with 4T1 tumor experiments and performed Rae1 qPCR analysis on lung melanoma tumor samples. S.L. performed TC1 tumor experiments on *Rag2*$^{-/-}$ mice and the histological analysis of NeuT^{+} mammary gland tumors. A.C., C.S.F., J.E., S. M., R.T., A.U., and B.M.K. developed the TAM small molecule inhibitor LDC1267 and characterized its kinase selectivity. S.W. and D.W performed Cbl-b qRT-PCR, ^{51}Cr-release NK cytotoxic assay, and perforin FACS analysis. R.N., S.J.C., T.G., R.H., and G.B., performed cell-free *in vitro* ubiquitylation experiments. W.Y.L. provided Cbl-b RING finger mutant mice. F.I., A.J. and J.P.F. provided reagents and expertise in key experiments. M.P. together with J.M.P. designed the experiments and wrote the manuscript.

Author Information. Reprints and permissions information is available at www.nature.com/reprints. Readers are welcome to comment on the online version of the paper.

The authors declare competing financial interests: the Lead Discovery Center GmbH (Dortmund) and Axel Ullrich (Munich) have patented the compound used in our study; Josef M. Penninger holds shares in a company that attempts to develop Cbl-b modulators.

Europe PMC Funders Author Manuscripts

substrates for Cbl-b. Treatment of wild-type NK cells with a newly developed small molecule TAM kinase inhibitor conferred therapeutic potential, efficiently enhancing anti-metastatic NK cell activity *in vivo*. Oral or intraperitoneal administration using this TAM inhibitor markedly reduced murine mammary cancer and melanoma metastases dependent on NK cells. We further report that the anticoagulant warfarin exerts anti-metastatic activity in mice via Cbl-b/TAM receptors in NK cells, providing a molecular explanation for a 50-year-old puzzle in cancer biology3. This novel TAM/Cbl-b inhibitory pathway holds the promise that it might be possible to develop a "pill" that awakens the innate immune system to kill cancer metastases.

Genetic ablation of *Cbl-b* or functional inactivation of its E3 ligase activity in mice results in $CD8^+$ T cell-mediated rejection of primary tumors in several different model4–6. In a control experiment subcutaneous injection of TC-1 tumor cells in $Cbl\text{-}b^{-/-}Rag2^{-/-}$, which lack B and T cells, caused a significant delay in tumor growth compared to $Cbl\text{-}b^{+/+}Rag2^{-/-}$ littermates (Fig. 1a), suggesting that innate immune cells are also involved. Immunohistochemistry revealed increased numbers of natural killer (NK) cells infiltrating the tumors of $Cbl\text{-}b^{-/-}$ mice (Extended Data Fig. 1a). Cbl-b is expressed in murine and human NK cells; expression levels were not altered in NK cells from E3 ligase defective mice ($C373A^{KI/KI}$), which carry a cysteine to alanine mutation at position 3737 (Fig. 1b, Extended Data Fig. 1b). Loss of Cbl-b expression ($Cbl\text{-}b^{-/-}$) or the $C373A^{KI/KI}$ mutation had no overt effects on NK cell development (Extended Data Fig. 1c,d).

$Cbl\text{-}b^{-/-}$ and $C373A^{KI/KI}$ NK cells exhibited significantly increased proliferation and IFN-γ production when activated *in vitro* and were also more efficient in killing RMA-S cells *in vivo* (Fig. 1c,d, Extended Data Fig. 1e-j). In contact with YAC-1 targets, $Cbl\text{-}b^{-/-}$ NK cells also displayed a higher capacity to kill, produce IFNγ, degranulate, secrete granzyme B, and to express higher levels of the cytotoxic mediator perforin; knockdown of Cbl-b in the human NK cell line NKL also resulted in enhanced cytotoxic towards Jurkat cells (Extended Data Fig. 2a-h). NK cell immunodepletion using NK1.1 Abs and functional blockade of NKG2D receptors abolished anti-TC-1 tumor responses in $Cbl\text{-}b^{-/-}$ and $C373A^{KI/KI}$ mice (Extended Data Fig. 3a-c). Moreover, subcutaneous B16F10 melanomas were slower growing in $Cbl\text{-}b^{-/-}$ and $C373A^{KI/KI}$ mice; depletion of $NK1.1^+$ cells reduced this increased survival of melanoma-bearing mice (Extended Data Fig. 3d-i). Thus, Cbl-b, via its E3 ligase activity, negatively regulates NK cell functions and controls NK-cell anti-tumor responses.

We next analyzed whether the absence of Cbl-b can potentiate the anti-metastatic activity of NK cells. Three weeks after i.v. B16F10 melanoma challenge, $Cbl\text{-}b^{-/-}$ and $C373A^{KI/KI}$ mice exhibited reduced lung metastases and increased survival (Fig.1e, Extended Data Fig. 4a-e). Immunodepletion of $NK1.1^+$ cells caused uncontrollable tumor growth in all $Cbl\text{-}b^{+/+}$, $Cbl\text{-}b^{+/-}$, $Cbl\text{-}b^{-/-}$, and $C373A^{KI/KI}$ mice (Fig. 1f,g). NKG2D blockade in $Cbl\text{-}b^{-/-}$ and $C373A^{KI/KI}$ mice also prevented the reduction of lung melanomas (Extended Data Fig. 4f-i). Of note, B16F10 melanoma by themselves do not express the NKG2D ligand Rae1, suggesting that this ligand is expressed on the tumor microenvironment. $Cbl\text{-}b^{-/-}$ and $C373A^{KI/KI}$ mice also exhibited significantly reduced metastases to extrapulmonary organs (Extended Data Fig. 5a-d). In the absence of NK cells, all $Cbl\text{-}b^{+/+}$, $Cbl\text{-}b^{+/-}$, $Cbl\text{-}b^{-/-}$, and $C373A^{KI/KI}$ mice displayed secondary metastases in multiple organs (Fig. 1h,i), even at lower tumor dose

(Extended Data Fig. 5e-g). Immunodepletion of $CD8^+$ T cells had no overt effect on the anti-metastases response of *Cbl-b*$^{-/-}$ and *C373A*$^{KI/KI}$ mice (Extended Data Fig. 5h,i). When backcrossed to perforin mutant mice (*Prf1*$^{-/-}$), *Cbl-b*$^{-/-}$*Prf1*$^{-/-}$ double-mutants were unable to reduce melanoma metastases (Fig. 1j,k; Extended Data Fig. 5j). Cbl-b has been implicated in anergic responses of NKT cells8, a cell type that also expresses NK1.19. To provide definitive proof that *Cbl-b* mutant NK cells directly reject metastatic melanomas, we set up a therapeutic transplantation model. Significantly fewer B16F10 metastases were observed in the lungs of wild-type mice that received *Cbl-b*$^{-/-}$ or *C373A*$^{KI/KI}$ NK cells, compared to untreated mice and mice receiving *Cbl-b*$^{+/+}$ NK cells (Fig. 2a-e). Thus, NK cells lacking Cbl-b, or defective in its E3 catalytic activity, are sufficient to inhibit the progression of lung melanomas and distant metastases.

To extend our findings to a spontaneous tumor metastasis model, *Cbl-b* mutant animals were crossed to *NeuT*$^+$ transgenic mice that develop metastatic breast tumors10. Although the onset of palpable mammary tumors was comparable, loss of Cbl-b markedly suppressed the growth of mammary tumors resulting in significantly prolonged overall survival (Extended Data Fig. 6a-d). Although the number of metastatic lung tumor foci was comparable between *Cbl-b*$^{+/-}$*NeuT*$^+$ and *Cbl-b*$^{-/-}$*NeuT*$^+$ mice, *Cbl-b*$^{-/-}$*NeuT*$^+$ mice showed a significant reduction of the tumor-to-lung area (Fig. 2f; Extended Data Fig. 6e-g). In *Cbl-b*$^{-/-}$*NeuT*$^+$ mice we observed a significant accumulation of NK cells within the metastatic foci (Fig. 2g; Extended Data 6h,i); depletion of NK cells with anti-asialo GM1 antibodies markedly enhanced metastases of mammary tumors into the lung of *Cbl-b*$^{-/-}$*NeuT*$^+$ and *Cbl-b*$^{+/-}$*NeuT*$^+$ mice (Fig. 2h-i; Extended Data Fig. 7a-e). Deletion of both or even one *Prf1* allele again abrogated the capacity of *Cbl-b*$^{-/-}$*NeuT*$^+$ mice to control mammary metastases to the lung (Extended Data Fig. 7f-h). Thus, *Cbl-b* deficient NK cells can also control metastatic tumors in oncogene-driven mammary cancer.

To identify ubiquitylation substrates, we performed an *in vitro* ubiquitylation reactions on 9000 human proteins. The transmembrane receptor tyrosine kinase TYRO3 was identified as the top candidate for CBL-B mediated ubiquitylation (Extended Data Fig. 8a). Tyro3, together with Axl and Mer constitute the TAM family of cell surface tyrosine kinase receptors11. In additional *in vitro* assays using recombinant proteins, we confirmed that CBL-B ubiquitylates all three TAM family proteins (Fig. 3a; Extended Data Fig. 8b). Activation of HeLa cells with GAS6, a known ligand for TAM receptors12, resulted in recruitment of Cbl-b to TAM receptors and Axl ubiquitylation; CBL-B knock-down using siRNA reduced GAS6-induced AXL ubiquitylation (Extended Data Fig. 8c,d). Thus, TAM receptors are molecular substrates for CBL-B ubiquitylation *in vitro* and *in vivo*.

In contrast to TAM triple mutant mice13, loss of Cbl-b had no overt effect on NK cell development (Extended Data Fig. 1c,d). The absence of Cbl-b, or its enzymatic E3 ligase activity, also had no apparent effect on basal Tyro3, Axl, or Mer surface expression in splenic NK cells (Extended Data Fig. 8e). Because TAM receptors can inhibit macrophage and dendritic cell activation14, we proposed that TAM receptors might also negatively regulate NK cells. Gas6 indeed suppressed proliferation and IFN-γ production of NKG2D-activated NK cells; *Cbl-b*$^{-/-}$ NK cells were resistant to this inhibition (Fig. 3b; Extended Data Fig. 8f). Mechanistically, whereas Gas6 stimulation resulted in downregulation of all three

TAM receptors from the cell surface, this downregulation was impaired in NK cells lacking Cbl-b (Fig. 3c). Impaired receptor downregulation was confirmed in HeLa cells using siRNA mediated CBL-B knockdown (Extended Data Fig. 8g,h). Thus, Cbl-b/TAM receptors constitute an inhibitory pathway for NK cell activation.

To assess whether modulation of this pathway could be used for anti-tumor immunotherapy, we developed a highly selective TAM kinase inhibitor, termed LDC1267. LDC1267 preferentially inhibits Tyro3, Axl, and Mer at low nanomolarity, as determined by tracer-based binding assays (Fig. 3d,e). Selectivity of LDC1267 was further assessed using a cell-free KINOMEscan assay covering 456 kinases (Fig. 3f, Supplementary Table 1). Cellular selectivity was confirmed employing a quantitative chemical proteomics approach, cell-based phosphorylation, and proliferation assays (Extended Data Fig. 9a-d). Treatment of NKG2D-activated NK cells with LDC1267 indeed abolished the inhibitory effects of Gas6 stimulation; LDC1267 had no apparent additional effect in *Cbl-b* deficient NK cells (Fig. 3g). *In vivo*, wild-type mice treated with LDC1267 showed enhanced cytotoxicity towards RMA cells overexpressing the NKGD2 ligand Rae-1 (RMA-Rae1) to the same extent as $C373A^{KI/KI}$ mice, but had no effect on the already enhanced NK cytotoxicity in *Cbl-b*-deficient mice (Fig. 3h; Extended Data 9e). To provide definitive proof that LDC1267 treatment can license NK cells to kill, we treated B16F10 melanoma-bearing mice with NK cells that were either untreated or treated *ex vivo* with our TAM inhibitor (Extended Data Fig. 9f). Adoptive transfer of LDC1267-treated wild-type NK cells significantly increased the anti-tumor response to levels observed in mice transplanted with $Cbl\text{-}b^{-/-}$ NK cells, but did not increase the anti-metastatic efficacy of *Cbl-b* knock-out NK cells (Fig. 3i), reinforcing the notion that Cbl-b acts downstream of TAM receptors for NK cell inhibition. These results indicate that TAM receptor inhibition using LDC1267 unleashes NK cells to kill tumors cells *in vivo.*

To test whether our novel TAM inhibitor can be used in an *in vivo* therapeutic setting, we challenged mice with B16F10 melanoma followed by intraperitoneal LDC1267 treatment. LDC1267 markedly reduced metastatic spreading of melanomas; NK1.1-depletion abolished the therapeutic benefits of LDC1267 (Fig. 4a-c). We next set-up an orthotopic metastatic breast cancer model, that is, injection of 4T1 breast cancer cells into the mammary fat pad of Balb/c mice15. LDC1267 treatment significantly reduced the numbers and sizes of 4T1 micro-metastases in the liver, without any apparent effect on the primary mammary tumor (Fig. 4d-f; Extended Data Fig. 10a-c). NK cell depletion using anti-asialo GM1 antibodies resulted in markedly enhanced 4T1 liver metastases and abolished the therapeutic benefits of LDC1267 (Fig. 4d-f). We finally tested whether LDC1267 could be also effective in the 4T1 liver metastasis model, when administrated orally (Extended Data Fig. 10d). Oral LDC1267 significantly reduced 4T1 liver micro-metastases (Extended Data Fig. 10e-g). Thus, using different model systems and different routes of administration, *in vivo* therapy with the TAM inhibitor LDC1267 consistently reduced metastases dependent on NK cells.

Warfarin is the most widely used oral anticoagulant worldwide16 and has been known to reduce tumor metastases in mouse and rat models3,17. The underlying mechanisms were largely speculative18,19. Besides its effects on coagulation, warfarin prevents γ-carboxylation of TAM ligands, rendering Gas6 unable to activate TAM receptors20. We

therefore hypothesized that warfarin could exhibit anti-cancer effects via modulation of the Gas6/TAM/Cbl-b pathway in NK cells. Administration of low dose warfarin, that inhibits TAM receptor activity *in vivo*21,22 without affecting coagulation, markedly reduced melanoma metastases to the lungs and distal organs of *Cbl-b*$^{+/+}$ and *Cbl-b*$^{+/-}$ mice but had no apparent effect on *Cbl-b* defective mice; the absence of NK1.1^{+} cells abolished the effects of warfarin on metastatic melanomas (Fig. 4g-j; Extended Data Fig. 10h-j). Moreover, warfarin treatment resulted in enhanced *in vivo* NK cell cytotoxicity towards their prototypic targets RMA-S and RMA-Rae1 (Extended Data Fig. 10k). Our data supports a coagulation-independent role of warfarin in tumor metastasis that relies on functional TAM receptors/Cbl-b in NK cells.

Our experiments uncover a novel inhibitory role of the E3 ligase Cbl-b in the regulation of NK cell functions via TAM receptors (Fig. 4k). Releasing the inhibition imposed by this TAM/Cbl-b pathway renders NK cells capable of rejecting tumor metastases. There is high redundancy for TAM receptor functions in immune cells23. Since all three TAM receptors are expressed on NK cells13, they most likely, as they do in NK cell development13, also exert redundant functions in NK cell activation. Indeed, genetic deletion of *Tyro3* alone did neither affect NK cell activation nor *in vivo* metastases control by NK cells (not shown). Mechanistically, upon ligand stimulation, Cbl-b is recruited to and ubiquitylates TAM receptors, which in turn appears to control TAM receptor internalization, corroborating the role of Cbl-b and its homologue c-Cbl in receptor tyrosine kinase endocytosis24. Of note, c-Cbl has been implicated in the ubiquitylation of Axl in human epithelial HLEC cells25. Whether Cbl-b affects NK cell activation solely via TAM receptors and/or also directly impinges on other receptor systems need to be determined.

Current tumor immunotherapies face the challenge of severe side-effects26. Since *Cbl-b* knock-out mice and mice treated with our TAM blocker do not exert any severe signs of inflammation or autoimmunity, there might be a therapeutic window for Cbl-b/TAM receptor inhibition to mediate tumor rejection without serious cytotoxicity. We also provide a molecular explanation for the longstanding conundrum on how warfarin confers anti-metastatic activity, offering the possibility to re-assess the use of vitamin K antagonists such as warfarin in cancer therapy. Importantly, the anti-tumor effects of our TAM inhibitor provide a proof-of-principle that it might be possible to develop a “pill” that awakens the innate immune system to kill cancer metastases.

Methods Summary

Cbl-b and *C373A*$^{KI/KI}$ mice have been previously reported7,27. Subcutaneous TC-1 and B16F10 tumors were induced by injection of 2.5x10^{5} tumor cells in the left flank of mice. For 4T1 tumors, 5x10^{5} 4T1 cells were inoculated directly into the third mammary fat pad. Mammary tumors and lung metastases in NeuT^{+} mice arise spontaneously10. For melanoma metastases, 2.5x10^{5} B16F10 cells were injected intravenously into the tail veins. Lungs were dissected for tumor quantification and the presence of metastases in any other organ was recorded. For adoptive transfer of NK cells, wild-type C57BL/6J recipient mice were inoculated i.v. with 2.5x10^{5} B16F10 at day 0, and one day later were either left untreated or inoculated i.v. with 1x10^{5} purified *Cbl-b*$^{+/+}$, *Cbl-b*$^{-/-}$, or *C373A*$^{KI/KI}$ *ex vivo* expanded NK

Europe PMC Funders Author Manuscripts

cells. For blocking TAM receptors, mice were orally treated in their drinking water with low doses of warfarin (0.5mg/ml). The TAM small molecule kinase inhibitor LDC1267 was developed applying rationale design based on the homology modeling and known non-specific TAM receptor kinase inhibitors. To study the therapeutic potential of TAM inhibition, *ex vivo* expanded and purified NK cells were treated for 2.5 hours with LDC1267 (2.5μM) or vehicle and i.v. injected into wild-type C57BL/6J recipient mice bearing B16F10 tumors. For 4T1 and melanoma metastases experiments, mice were treated with LDC1267 using daily oral gavage (100mg/kg) or intraperitoneal injections (20mg/kg). All tumors were quantified blindly based on a histomorphometric analysis using the Definiens Developer XD image analyser software.

Methods

Mice

Cbl-b$^{-/-}$ mice were generated in our laboratory27. Cbl-b E3 ligase-defective -*C373A*$^{KI/KI}$- knock-in mice were described previously7. *Rag2*$^{-/-}$ mice were obtained in-house. *Prf1*$^{-/-}$ and *NeuT*$^{+}$ transgenic mice were a kind gift of R. Zinkernagel/H. Hengartner (Switzerland) and G. Forni (Italy), respectively. *Tyro3*$^{-/-}$ mice were purchased from The Jackson laboratory. All experimental procedures were performed on mice backcrossed for at least 7 generations onto the Balb/c (for NeuT^{+} and 4T1 mammary tumor experiments) or C57BL/6J background (for all other experiments). If not otherwise stated, only 7-12 weeks old, sex- and age-matched littermate mice were used. For simplification we show *Cbl-b*$^{+/+}$ controls for *Cbl-b*$^{-/-}$ and *C373A*$^{KI/KI}$ mice; in all results reported, similar results were obtained with the exact littermate controls. All animal experiments were carried out according to an ethical animal license protocol complying with the current Austrian law.

Flow Cytometry

Single cell suspensions were immunostained for 30 minutes at 4°C in FACS buffer (PBS-2% FCS). Fc-receptors were blocked with anti-CD16/32 antibodies (BD Pharmingen). For staining of NK cells, directly labeled antibodies against NK1.1, DX5, CD3ε, Ly49-F, Ly49-D, Ly49I/C, NKG2A/C/E (all from BD Pharmigen), and NKG2D, NKp46, CD27, CD11b, CD122, CD43, Ly49A (eBioscience) were used. For detecting NKG2D ligands antibodies against Rae1 (pan-specific) and Mult1 were used (both from R&D systems). Tyro3, Axl and Mer surface expression was detected using goat antibodies (all from R&D Systems) followed by Alexa 488 anti-goat secondary antibodies (Life Technologies™). Control goat isotype antibodies (R&D Systems) and *Tyro3*$^{-/-}$ NK cells were used as controls. Data was acquired using a multi-colour flow cytometer (FACSCanto™ or FACSFortessa™, BD) equipped with the FACSDiva™ software (BD). Data analysis was performed using FlowJo™ software (Tree Star).

Western blotting and immunoprecipitations

Proteins from purified murine NK cells, the human NK92 cell line (a gift from E. Vivier, Marseille) and HeLa cells were extracted using a protein lysis buffer (0.5% NP-40, 150 mM NaCl, 50mM Hepes pH 7.8, 1mM EDTA pH 8) containing protease inhibitors (Thermo Scientific). 20-40μg of tissue lysate were resolved on a 4-12% SDS-PAGE, electro-

transferred to polyvinylidene difluoride membranes, and probed with anti-Cbl-b (SantaCruz Biotec, sc-8006) or anti- Tyro3 (kind gift from Anne. L. Prieto) antibodies and as loading control anti-β-actin, anti-GAPDH, or anti-β tubulin (Cell Signaling Technology) according to standard procedures. For Gas6 and Cbl-b co-immunoprecipitations, HeLa cells were serum-starved overnight and stimulated at 37°C with 450ng/ml recombinant His-tagged murine Gas6 (R&D System) for different time periods, and then lysed as described above. 400μg of total protein lysates were immunoprecipitated overnight at 4°C with 25μl of HisPur cobalt resins (Thermo Scientific) and eluted by boiling at 95°C for 5 minutes in reducing loading buffer. Immunoprecipitated and input samples were run on SDS-PAGE gels, transferred to polyvinylidene difluoride membranes and blotted for Cbl-b.

qRT-PCR

Total cellular RNA was extracted from FACS-sorted primary murine and human NK and T cells using Tri-Reagent (Sigma). Total RNA (1 μg) was reverse-transcribed to cDNA by using a high Capacity cDNA Reverse Transcriptions Kit (Applied Biosystems). cDNA was then amplified via real-time PCR on an ABI PRIM 7000 Sequence Detection System (Applied Biosystems) with TaqMan gene-expression kits for mouse and human Cbl-b and as a normalization control GAPDH (Applied Biosystems). For the detection of Rae1 expression in melanoma lung tumors, RNA samples were purified from dissected healthy lungs and melanoma lung tumors using the Qiagen RNeasy Mini Kit and including DNase I digestion to avoid potential DNA contamination. 1 μg of total RNA was reversed transcribed using SuperScript II Reverse Transcriptase Kit (Invitrogen) and oligo-dT primers. Rae1 expression levels were quantified by real-time quantitative PCR (iCycler iQ BioRad) using the iQ SYBR Green Supermix from BioRad, and normalized to Pum1 mRNA levels. Rae1-F: TGCCATCGATCCAACGGTACl; Rae1-R: TGGTCCTGGCATCTTTGTCC.

Lymphokine activated killer cell (LAK) cultures

For generation of *ex vivo* expanded NK cells (LAK), splenocyte suspensions were enriched for NK cells by $DX5^+$ magnetic separation (MACS®, Miltenyi Biotec) and cultured in RPMI media containing 10% FCS (Gibco), 100 IU/ml penicillin-streptomycin, 2 mM glutamine, 1mM Na-pyruvate, 1% MEM non-essential amino acids, 30μM β-mercaptoethanol (all from Sigma), and 100ng/ml IL-15 (Peprotech). After 5-7 days incubation, LAK cultures were highly enriched in $NK1.1^+$ $CD3\varepsilon^-$ cells (70-85%) as determined by FACS. For Western blot analysis and adoptive transfer experiments, NK cells ($NK.1.1^+$ $CD3\varepsilon^-$) were purified using the FACSAria cell sorter (BD Bioscience). For *in vitro* NK cell assays, and to assure equal numbers of NK cells were present in each sample, NK cells were either sorted or the percentage of NK cells for each LAK culture was determined by FACS and adjusted accordingly.

In vitro NK cells studies

For NK cell proliferation studies, $1x10^5$ NK cells sorted from LAK cultures were stimulated in replicates in 96 U-bottom wells pre-coated with serial concentrations of anti-NK1.1 (clone PK136) or anti-NKG2D (clone MI-6) activating antibodies. To study the role of TAM receptors in NKG2D-mediated NK cell proliferation, NK cells were stimulated with 30μg/ml of plate-bound anti-NKG2D activating antibodies in the presence of serial

concentrations of soluble recombinant mouse Gas6 (R&D Systems). Proliferation was measured after 72 hrs either by scintillation counting after an overnight pulse -at 56 hours- with 1 μCi of $^{[3H]}$thymidine or by BrdU incorporation in a colorimetric ELISA (Roche), and further verified by absolute cell numbers quantification and by FACS analysis using a cell tracer (Cell Trace™ Violet, Molecular Probes). For IFN-γ production, B-cell depleted splenocyte suspensions from poly I:C treated mice (200μg/mice, added 16 hrs prior to cell harvesting), as well as *ex vivo* expanded NK cells were stimulated in triplicates (1-2x10^5/well) for 5 hrs with serial concentrations of plate-bound anti-NK1.1 or anti-NKG2D antibodies, in the presence of GolgiPlug (BD Bioscience). To implicate TAM receptors, serial concentrations of soluble recombinant mouse Gas6 (R&D Systems) were added. Cells were then stained with antibodies against CD3ε and NK1.1 (for NKG2D stimulation) or CD3ε and DX5 (for NK1.1 stimulation), fixed and permeabilized, intracellularly stained with anti-IFN-γ antibodies (Pharmingen), and analyzed by flow cytometry. For NK cell degranulation, *ex vivo* expanded NK cells were incubated in replicates with YAC-1 cells at an effector:target ratio of 5:1. After 1 hour, cells were stained with antibodies against NK1.1, CD3ε, and LAMP-1 (all Pharmingen) and the frequency of degranulating NK cells (LAMP-1^+ NK1.1^+CD3$ε^-$) was determined by FACS and corrected for spontaneous degranulation (effector:target ratio of 1:0). Granzyme B release was determined by ELISA (R&D Systems) in the supernatant of *ex vivo* expanded NK cells co-cultured for 4hrs with YAC-1 cells at different effector:target ratios. To determine the frequency of perforin-secreting NK cells, cells were stimulated with YAC-1 cells at an effector to target ratio of 2:1 in the presence of monensin (Golgi-Stop, BD Biosciences). After 6 hrs, samples were stained for NK1.1 and CD3ε surface expression, fixed and permeabilized (BD Pharmingen), intracellularly stained for perforin (eBioscience), and analysed by FACS.

NK cytotoxicity assays

FACS-based *in vitro* cytotoxic NK cell assays were performed as described28. Briefly, YAC-1 target cells were labeled with the PKH26 dye (PE channel, Sigma-Aldrich) and cultured in triplicates with different ratios of *ex vivo* expanded effector NK cells. After 4 hrs, cells were stained with the viability probe TO-PRO-3 iodide (APC channel, Invitrogen) and NK cytotoxicity was determined by FACS analysis as the percentage of dead YAC-1 cells (PE$^+$APC$^+$). Dye toxicity and/or spontaneous YAC-1 cell death were controlled in the absence of effector cells and never exceeded 3%. For radioactive chromium (^{51}Cr) release assays, YAC-1 and Jurkat *t*arget cells were labeled for 1 hr at 37°C with 100 ¼Ci $Na_2Cr^{51}O_4$ (specific activity 300 to 500 Ci/g chromate; Hartmann Analytic, Germany), resuspended at a concentration of 5x10^4 cells/ml, and then co-incubated in triplicates (96-wells, 200μl) with murine NK cells or human NKL cells at various effector:target (E:T) ratios. After 4 hrs, the supernatant was harvested and the percentage of ^{51}Cr specific release calculated using the standard formula: % cytotoxicity = 100 x (sample release–spontaneous release)/(100% killed release–spontaneous release). Delivery of chemically synthesized short interfering RNA (siRNA) into human NKL cells was accomplished by using the Amaxa Nucleofector system and human NK-cell Nucleofector Kits from Lonza Group Ltd (Basel, Switzerland) according to the manufacturer's recommendations. Cbl-b siRNAs were from Dharmacon RNA Technologies (Human #10 5'-UUUGCUAACGG ACCAGUACUU-3´ and Human #11 5'-UAAUACCCAAAAUUCGACCUU-3´). For assessing NK cytotoxicity *in vivo,* RMA-S

and RMA cells were labeled at 37°C for 5-10 minutes with CFSE (Molecular Probes) and eFluor®670 (eBioscience), respectively, mixed in a 1:1 ratio and injected intraperitoneally ($1x10^7$ per mouse). For assessing NKG2D-mediated NK cell cytotoxicity *in vivo*, NK-cell resistant RMA cells and NK-sensitive RMA cells expressing NKG2D ligands (RMA-Rae1)29 were used. 24 hrs later, cells were recovered by peritoneal lavage and the relative percentage of sensitive and resistant target cells determined by flow cytometry on gated live cell populations (DAPI negative).

Tumor experiments

Of note, only the first TC-1 tumor experiment shown in Fig. 1a was performed in *Rag2*$^{-/-}$ backgrounds. All other tumor experiments were performed in Rag2 sufficient mice and the relevance of NK cells was assessed by immunodepletion approaches and/or NK cell transplant experiments. For subcutaneous tumor models, $2.5x10^5$ TC-1 or B16F10 cells were s.c. injected into the shaved left flank of 8-12 wks old female mice under anesthesia. Tumor growth was monitored 3 times per week with a caliper, and mice were euthanized when tumor reached $1cm^3$ in accordance with animal license protocols. For metastatic melanoma studies, mice were intravenously injected into the tail vein with $2.5x10^5$ B16F10 cells and euthanized 3 weeks later (at day +21). To better assess the quantitative effect of NK cells in Cbl-b-dependent B16F10 tumor rejection, untreated and NK1.1$^+$-cell depleted mice were challenged with B16F10 cell using a 10 times lower dose ($2.5x10^4$) and longer periods of time (day +28). To study early tumor responses, mice were i.v. inoculated with $7.5x10^5$ B16F10 cells and euthanized at day+7. At the endpoint of each experiment, mice were euthanized, lungs were collected to determine the relative tumor-to-lung ratios and a careful macroscopic examination of all internal organs was performed to detect the presence of B16F10 extrapulmonary metastases. The prevalence of extrapulmonary metastases for each cohort is defined as the proportion of mice in each cohort showing B16F10 tumor metastasis in other organs than the lung, regardless of the number of organs affected. For mammary tumor studies, mammary gland palpation of NeuT$^+$ transgenic mice started at day +75 after birth. Tumor growth in all mammary glands was monitored every 5-7 days with a caliper. Mice were euthanized when the total volume of all mammary tumors $\geq 1.5cm^3$. At this point, mammary tumors and lungs were collected, fixed and sectioned to assess tumor growth and lung metastases. Since TC-1 and 4T-1 cells are derived from female mice, only female animals were used for TC-1 and 4T-1 tumor models. Similarly, to study spontaneous mammary tumor metastases only NeuT$^+$ transgenic female mice were used. In all cases, only mice carrying tumors were included in the analysis. Tumor quantification, as described below, was performed blindly. However, for tumor inoculation we were not blinded.

Therapeutic transfer of NK cells into melanoma bearing mice

At day 0, recipient *wild-type* C57BL/6J mice intravenously received $2.5x10^5$ B16F10 melanoma cells. One day later, NK1.1$^+$CD3ε$^-$ *Cbl-b*$^{+/+}$, *Cbl-b*$^{-/-}$, and *C373A*$^{KI/KI}$ NK cells were sorted from the corresponding LAK cell cultures and adoptively transferred to recipient mice (100.000 cells i.v. per mouse). A control group did not receive LAK cells. Control and NK-cell transplanted mice were euthanized at day +14 post–tumor inoculation and lungs were harvested and dissected to determine the number of tumor foci and the relative tumor

volume. In addition, the presence of macroscopically visible extra-pulmonary metastasis was recorded.

Quantification of tumors

For the quantification of B16F10 melanoma metastases, lungs were harvested and photographed (two lung images per mouse, one per each lung "side") using a stereomicroscope (Leica MZ APO). For the quantification of metastatic NeuT$^+$ mammary carcinomas, lungs isolated from mice bearing NeuT$^+$ mammary tumors (each mouse with a total mammary tumor volume ≥1.5cm^3 to control for the size of the primary tumor) were paraffin-embedded and micro-sectioned at three different planes (~ 350μm apart) and stained with haematoxylin-eosin (H&E). Histological slides (three per mouse) were then scanned on a Mirax Scanner (Zeiss). Tumors in each image were quantified based on a histomorphometric analysis performed automatically using the Definiens image analyser software (Definiens AG, http://www.definiens.com). An algorithm was programmed and executed using this software to discriminate, mark, and calculate the number and total area (as pixel) of tumors and "healthy" surrounding tissue. To assure precision, each image processed by the software was then inspected blindly by 2 independent scientists (for the B16F10 experiments) or a trained pathologist (for NeuT$^+$ tumors). To highlight the precision of this selection please see Extended Data Fig. 4a, 8a and 13b.The quantification of tumors in each image is relative to the total tissue area and is presented as a percentage, i.e. tumor-to-lung ratio = [tumor area (pixel)/tumor+healthy surrounding tissue area (pixel)]x100.

Depletion and blocking of immune cells in tumor-bearing mice

Depleting antibodies against CD8 (clone 24.3) and NK1.130 (clone PK136) as well as NKG2D blocking antibodies (clone MI-6)31, were produced in-house by hybridoma cultures. The stocks were kindly provided by C. M. Melief, Leiden (CD8 and NK1.1), and David H. Raulet, Berkeley (NKG2D). Anti-Asialo GM1 antibodies were obtained commercially (WAKO). For CD8$^+$ and NK1.1$^+$ cell depletion, mice were intra-peritoneally (i.p.) injected 4 and 2 days before tumor inoculation with 50 μg of anti-CD8 or 100μg of anti-NK1.1 depleting antibodies, respectively. Treatment continued every 5 days after tumor inoculation until the experimental endpoint. For blocking NKG2D *in vivo*, mice were injected i.p. with 200μg of anti-NKG2D blocking antibodies 6 and 3 days before tumor inoculation, and twice a week after tumor inoculation until the endpoint of the experiment. Since NK1.1 receptors are not expressed in the Balb/c genetic background32, depletion of NK cells in *NeuT*$^+$ and 4T1 tumor models (on a Balb/c background) was accomplished by i.p. injection of anti-asialo GM1 antibodies33, according to manufactures' instructions (WAKO). Administration of anti-asialo GM1 Abs was initiated when total mammary tumor volume reached 10-100mm^3 and continued every 5 days until the endpoint of the experiment. In all cases, control groups were left untreated and cell-specific depletion and NKG2D blocking were confirmed in spleen and blood samples by FACS analysis at day 0 and at the endpoint of each experiment.

Immunohistochemistry

Detection of NK cells was performed with anti-NKp46 antibodies (R&D system) using the automated Leica BOND-III System (Leica Biosystems). The specificity of this antibody has

been previously demonstrated34 and was further controlled in every round of staining by using spleen and lung samples of control and NK-cell depleted mice. TC-1 tumors and lungs from B16F10 and NeuT$^+$ tumor-bearing mice were fixed overnight in 4% formalin, paraffin-embedded, and micro-sectioned at two or three different planes (more than 350μm apart). Slides were scanned on a Mirax Scanner (Zeiss) and analyzed using the Definiens Tissue Studio software (Definiens AG). All tumor areas in each section were analyzed and every intratumoral cell was classified as positively or negatively stained. For each mouse 2 to 3 tissue slides at different intervals were analyzed. The quantification of NKp46$^+$ cells is relative to the total intratumoral cell numbers and is presented as a percentage = [(number of positive cells/total intratumoral cell number)x100]. The representative images shown in the figures were acquired using the Panoramic Viewer Software (3DHistech Ltd.).

Identification of Cbl-b ubiquitylation targets

In vitro ubiquitylation arrays were performed by Invitrogen (ProtoArray Ubiquitin Ligase Identification Profiling Service, USA). Protoarray ® Human Protein Microarrays containing over 9000 proteins were incubated with purified ATP, E1 activating enzymes (100nM), HA-Ub (100μg/ml), the E2 UbcH5b (1μM) and either wild-type Cbl-b or C373A mutant Cbl-b (100nM, in duplicates). To control for ubiquitylation-independent signals, an array was incubated just with detection antibodies (negative control). To exclude E2-specific ubiquitylation substrates, an array was run with all reagents and enzymes except for the E3 ligase (Cbl-b). Ubiquitylation substrates were detected with mouse anti-HA antibodies followed by fluorescently labeled anti-mouse antibodies. Arrays were then scanned and pixel intensity data for each protein spot was acquired using GenePiX software. A comparative analysis of the relative fluorescent signal of every spot in each array allowed the identification of putative Cbl-b ubiquitylation substrates.

In vitro ubiquitylation assays

To confirm the array data, cell-free *in vitro* ubiquitylation assays were performed. Briefly, full length FLAG-tagged human Tyro3, Axl, and Mer (all from Origene) were incubated at 30°C for 1 hour in a reaction mixture (20 μl) containing ubiquitylation solution (Enzo Biomol), 1 μM ATP, 1 mM DTT, 20 U/ml inorganic pyrophosphatase, 5 mM Mg-ATP, 2.5 μM of ubiquitin (Enzo Biomol), 100 nM of His-Uba1 (home-made), 2.5 μM of UbcH5B (Enzo Biomol), and 100 nM of full length human Cbl-b (Novus Biologicals). As a control, the same reactions were performed in the absence of recombinant Cbl-b. The reaction was quenched by adding 20 μl of 2 times reducing gel loading buffer and heating at 95°C for 5 min. Finally, the samples were immunoblotted with anti-Ubiquitin (sc-8017, SantaCruz Biotec) or anti-FLAG antibodies (Sigma). For loading controls, samples were blotted with anti-Cbl-b (sc-8006, SantaCruz Biotec.) and anti-FLAG antibodies (Sigma).

Ubiquitination of Axl in HeLa cells

Delivery of chemically synthesized short interfering RNA (siRNA) into HeLa cells (gift from Juan. P. Fededa) was performed using Lipofectamine® RNAiMAX Transfection Reagent (Sigma), ON-TARGETplus SMARTpool for Human Cbl-b, and as control an ON-TARGETplus NON-targeting Pool (both from Thermo Scientific, L-003004-00-0005 and D-001810-10-05) according to manufacturer's protocol. Cbl-b knockdown was verified by

Western blotting. 48hrs post-siRNA transfection, HeLa cells were serum-starved overnight and then stimulated at 37°C with 500ng/ml recombinant human Gas6 (R&D Systems) for different time periods. Cells were then placed on ice, washed in ice cold PBS and lysed in RIPA buffer (Sigma) containing protease inhibitors (Thermo Scientific) and 10mM N-Ethylmaleimide (Sigma). 600-1000μg of total protein lysates were immunoprecipitated overnight at 4°C with 4μg anti-Axl antibodies (Santa Cruz Biotec sc-1097) and 25μl of recombinant Protein G-Sepharose 4B conjugates (Invitrogen). After 4 washes, elution from the beads was performed by adding 20 μl of 2 times reducing gel loading buffer and heating at 95°C for 5 min. Immunoprecipitated and input samples (45μg) were run on SDS-PAGE gels, transferred to nitrocellulose membranes and blotted with anti-Ubiquitin (P4D1, sc-8017) and anti-Axl (sc-1097) antibodies in 5%BSA-TBS-Tween according to standard protocols.

TAM receptor internalization

Receptor internalization was performed following a protocol described previously35. Briefly, freshly isolated mouse splenocytes and HeLa cells (serum starved for 16 hours) were incubated on ice for 1 hour with 200ng/ml of recombinant mouse or human Gas6, respectively (R&D Systems). After washing, cells were resuspended in 0.2% BSA medium and incubated at 37°C for the indicated time periods. Cells were then placed on ice, washed with ice-cold PBS, incubated 5 minutes with cold acidic buffer to remove any bound ligand (100mM NaCl, 50nM glycine, pH=2.5), and subsequently washed twice in cold PBS. HeLa cells were mechanically detached using a cell-scraper. Cell suspensions were then stained on ice for 45 minutes with anti-Axl, anti-Tyro3, anti-Mer, and a control goat isotype antibodies (all from R&D Systems) in 0.2% BSA-PBS containing 0.1% sodium azide, followed by incubation with anti-goat Alexa-488 secondary antibodies. Splenocyte suspensions were also stained for anti-NK1.1 and anti-TCRβ (BD Bioscience) and DAPI (Sigma). Receptor internalization analysis was performed by FACS on gated viable NK cells ($DAPI^-$ $NK1.1^+TCR\beta^-$ cells) or gated viable HeLa cells ($DAPI^-$). The amount of receptor present at the cell surface at each time point-point is displayed as a percentage of the relative FITC Mean Intensity value in relation to the control 0 minute time point (=100% surface expression).

Generation of the TAM receptor tyrosine kinase inhibitor LDC1267

LDC1267 was rationally designed as type II kinase inhibitor using a pharmacophore-based back pocket approach. Hundreds of compounds from the series of quinolines were synthesized and optimized using a cell-based Axl autophosphorylation assay as the primary enzymatic read-out. The synthesis of the chemical series of 1-nitrogen-heterocyclic-2-carboxamides including the current lead N-(4-((6,7-dimethoxyquinolin-4-yl)oxy)-3-fluorophenyl)-4-ethoxy-1-(4-fluoro-2-methylphenyl)-1H-pyrazole-3-carboxamide (LDC1267) has been recently reported36. LDC1267 was synthesized as follows: To a solution of 4-ethoxy-1-(4-fluoro-2-methyl-phenyl)pyrazole-3-carboxylic acid (127mg, 0.48mmol, 1.5eq.) in dry DCM (2mL) at 0°C was added slowly oxalyl chloride (63uL, 0.72mmol, 2.3eq.) and a drop of dry DMF (10μL). The cooling bath was removed and the mixture was stirred for 1.5h at room temperature. Solvents were removed in vacuo, the crude material resolved in dry toluene and evaporated under reduced pressure to yield the acid

chloride. The acid chloride was solved in dry pyridine (2mL) at 0°C and 4-((6,7-dimethoxyquinolin-4-yl)oxy)-3-fluoroaniline (100mg, 0.32mmol, 1.0eq.) was added. After stirring for 2 hours at RT, water was added and solvents were removed under reduced pressure. The crude product was purified by flash chromatography on silica gel (DCM/MeOH = 100:0 to 5:1) to yield the desired product LDC1267 (136mg, 0.24mmol, 76%). In order to prepare the HCl-salt, LDC1267 (125mg) was solved in ACN (3mL) and water (3mL). After adding aq. HCl-sol. (c=1mol/L, 0.22mL, 1.0eq.) and stirring for 1 hour, the mixture was lyophilized yielding the HCl-salt of LDC1267 (132mg). ^{1}H NMR (400MHz, d_6-DMSO, 300K) δ 1.34 (t, *J* = 7.0 Hz, 3H), 2.23 (s, 3H), 4.01 (s, 3H), 4.02 (s, 3H), 4.03 (q, J = 7.0 Hz, 2H), 6.94 (d, *J* = 6.5 Hz, 1H), 7.19 (td, *J* = 8.5, 2.9 Hz, 1H), 7.29 (dd, *J* = 9.7, 2.9 Hz, 1H), 7.49 (dd, *J* = 8.8, 5.4 Hz, 1H), 7.54 (t, *J* = 9.0 Hz, 1H), 7.75 (m, 3H), 8.02 (s, 1H), 8.10 (dd, *J* = 13.3, 2.4 Hz, 1H), 8.79 (d, *J* = 6.5 Hz, 1H), 10.23 (s, 1H). MS (ES) $C_{30}H_{26}F_2N_4O_5$ requires: 560, found: 561 $(M+H)^+$.

To establish the inhibitory profile of LDC1267, this compound was extensively tested using three selectivity assays to define its biochemical and cellular selectivity. Firstly, we accessed a broad kinase inhibition panel of 456 kinases (including 66 natural occurring kinase mutations; conducted by DiscoverX, San Diego, USA). 39 out of 456 tested kinases were inhibited to a lower than 10% remaining activity at 1μM concentration of LDC1267. Thus, at the level of a cell-free assay, LDC1267 inhibits less than 10% of the tested kinome at a concentration which is roughly 100 times higher than the IC_{50} value for Axl. Secondly, we tested the cellular selectivity of LDC1267 by employing a quantitative chemical proteomics approach37,38. Lysates from Hs578t cells were incubated with an unspecific kinase inhibitor covalently bound to a matrix (experiments were conducted by Kinaxo/Evotec, Martinsried, Germany). Elution with up to 10μM LDC1267 identified two high affinity protein targets (K_D about 30nM), namely Axl and Met. This correlates well with the cellular inhibition of Axl phosphorylation using LDC1267 in these cells (IC_{50} value is ~0,010μM). Of not, Tyro3 is not expressed in Hs578t cells. In addition, MAP2K5, Abl, Fer, and Src bound to the matrix as well, but with approximately 10-fold lower affinity. Other kinase targets, which were identified in the cell-free KINOMEscan selectivity assay as LDC1267 binders (Aurora, Lck, DDR1, LOK, BLK, MAP4K5, or CDK8) did not bind the kinase inhibitor matrix, although they are expressed in Hs578t cells. Similarly, kinases such as DDR2, Mst1, Plk4, Slk and Tec, also identified in the KINOMEscan experiment with reduced affinities (≤20% remaining activity at 10μM LDC1267), did not bind to LDC1267 in our chemoproteomics experiment. This demonstrates that LDC1267 is even more selective at the cellular level when compared to its biochemical profile.

Thirdly, we investigated the effects of LDC1267 (up to 30μM) on proliferation of 95 different cancer cell lines. LDC1267 did not affect proliferation of 84 cell lines and moderately affected proliferation of 11 cell lines (best IC_{50} value at ~ 5μM; average IC_{50} value for those 11 cell lines is ~15μM). We also tested more than 1500 different kinase inhibitors in the same panel of cancer cell lines. In these assays non-specific kinase inhibitors like staurosporine or dasatinib inhibit proliferation of (nearly) every cell line with IC_{50} values below 0.1μM. By contrast, specific kinase blockers inhibit proliferation of only a few cell lines (e.g. K562 cells in the case of imatinib). LDC1267 does not affect cell

proliferation at all at a concentration >1 μM, a concentration at which in all our assays TAM receptor tyrosine kinases are completely blocked.

Thus, LDC1267 is a highly selective kinase inhibitor binding to the TAM receptor tyrosine kinases and c-Met. Finally, we compared the cellular specificity/activity of LDC1267 and 15 close chemical analogs for Axl or c-Met using cell-based phophorylation assays. The biochemical Axl Kd values were in the same range as the cellular IC_{50} values for Axl autophosphorylation. In contrast, this was not observed for c-Met. LDC1267 and close analogs had cellular c-Met autophosphorylation IC_{50} values about one order of magnitude higher than the biochemical values. Therefore, the inhibition of Axl by LDC1267 can be numerically directly translated into Axl inhibition in cells, whereas a similar effect on c-Met autophosphorylation requires 10-fold higher concentrations indicating an additional cellular specificity for LDC1267. Thus, LDC1267 is a highly selective inhibitor for TAM receptor tyrosine kinases with a type II binding mode (tight binding with slow K_{on} and K_{off} rates).

Kinase binding assays

For optimization of Axl/TAM receptor inhibitors, an Axl binding assay was established (HTRF method; Kinase tracer 236). This assay is based on the binding and displacement of the Alexa Fluor 647-labeled Kinase tracer 236 (Life Technologies) to each GST-tagged kinase used in the binding assay. Binding of the tracer to the kinase was detected by using Europium (Eu)-labeled anti-GST antibodies. Simultaneous binding of both the fluorescent tracer and the Eu-labeled antibodies to the GST-tagged kinase generates a FRET-signal. Binding of inhibitor to the kinase competes for binding with the tracer, resulting in a loss of the FRET signal. For the assay, the compound was diluted in 20 mM Hepes pH 8.0, 1 mM DTT, 10 mM $MgCl_2$ and 0.01 % Brij35. Then, the kinase of interest (5nM final concentration), fluorescent tracer (15nM final concentration; purchased from Invitrogen, Darmstadt/Germany), and LanthaScreen Eu-anti-GST antibody (2nM final concentration; purchased from Invitrogen, Darmstadt/Germany) were mixed with the respective compound dilutions (from 5 nM to 10 μM) and incubated for 1 hour. The FRET signal was quantified using an EnVision Multilabelreader 2104 (Perkin Elmer).

Comparing the results for more than 200 compounds in the HTRF assay with the results from cellular phosphorylation assays for Axl/TAM receptor kinase inhibitors from different structural classes revealed a clear correlation for the two assay formats. Reference compounds such as BMS-777607/ASLAN002, sunitinib, and staurosporine showed inhibitory activities as expected. Most importantly, we observed almost no numerical shift in activity when using either the biochemical HTRF method or the cellular autophosphorylation assay for measuring Axl activity. This indicates that LDC1267 binds with a mode of action which is independent of the ATP concentration (1 to 5mM ATP present in cells). Based on the published structure of BMS-777607 with Axl kinase (PDB3f82) we have established a homology model and investigated the binding mode of our compounds. Compounds from the quinoline series such as LDC1267 were shown to bind in a BMS-777607-like mode to Axl, further indicating a type II binding mode.

LDC1267 studies on NK cells

For IFNγ studies, *ex vivo* expanded *Cbl-b*$^{+/+}$ and *Cbl-b*$^{-/-}$ NK cells were pre-treated with vehicle (DMS0) or LDC1267 (2.5μM) for 2.5 hours, and then stimulated in triplicates (1-2x10^5/well) with 30μg/ml of plate-bound anti-NKG2D antibodies in the presence of GolgiPlug (BD Bioscience) and in the absence or presence of recombinant mouse Gas6 (400ng/ml, R&D Systems). After 5 hours incubation, IFNγ production was determined by FACS analysis on NK1.1$^+$CD3$^-$ cells. For *in vivo* NK cell cytotoxicity studies, *Cbl-b*$^{+/+}$ and *Cbl-b*$^{-/-}$ mice were treated 3 times –12 hours apart- by oral gavage with vehicle (70% PEG400:30% H2O) or 100mg/kg LDC1267 before the intraperitoneal inoculation of a mixture of differentially labeled RMA:RMA-Rae1 cells. 24 hours after inoculation cytotoxicity towards RMA-Rae1 cells was analyzed as described above. For adoptive NK cell transfers, wild-type C57BL/6J recipient mice were inoculated i.v. with 2.5x10^5 B16F10 melanoma cells at day 0. At days +1 and +4, syngeneic C57BL/6J NK1.1$^+$CD3ε$^-$ *Cbl-b*$^{+/+}$ and *Cbl-b*$^{-/-}$ NK cells were FACS sorted from the corresponding LAK cell cultures (5 days of culture) and either treated with vehicle (DMSO) or incubated with LDC1267 (2.5μM) for 2.5 hours. Vehicle and LDC1267-treated *Cbl-b*$^{+/+}$ and *Cbl-b*$^{-/-}$ NK cells were then washed and transplanted intravenously to recipients (1x10^5 cells/mouse). A group of recipient mice that did not receive LAK cells served as a control. Mice were euthanized at day +14 to quantify lung melanoma metastases using the Definiens software.

4T1 metastasis model

4T1 metastatic mammary cancer cells, that form micro-metastases in the liver and lung, have been previously reported15. Briefly, 4T1 tumor cells were orthotopically injected into the third mammary fat pad (5x10^5 cells, re-suspended in matrigel) of 9-12 weeks-old syngeneic wild-type Balb/c female mice. Tumor growth in the mammary fat pad was monitored using a caliper. LDC1267 and vehicle treatment was initiated in animals that developed palpable primary mammary tumors (day +6, with an average tumor volume of 83mm^3 at the start of inhibitor administration). *In vivo* LDC1267 treatment was performed every 12 hours via oral gavage (BID:100mg/kg) or i.p. administration (20mg/kg). 12 hours after the last dose, LDC1267 plasma concentrations were measured using LCMS-based analytics. Control mice were treated with vehicle (70% PEG400:30% H2O for oral gavage or 90% PEG400:10% DMSO for i.p. administration). For studying the dependence of NK cells in this 4T1 tumor model, NK cells were depleted using anti-asialo GM1 Abs starting at day -5 prior to tumor inoculation. Injections of the depleting Abs were continued every 5 days until the experimental endpoint. Micro-metastases into the lung and liver were analyzed at day +21 (for oral gavage treatment) and day +16 (for i.p. treatment) after initial 4T1 challenge. Livers and lungs were paraffin-embedded, micro-sectioned, H&E stained and scanned on a Mirax Scanner (Zeiss). For this particular tumor quantification in the liver and to exclude inflammatory foci, a manual selection was preferred instead of an automated one. Using the Definiens Developer XD Software a trained animal pathologist established the number and relative tumor area of 4T1 micro-metastasis in each tissue section. For this, 10-22 different image fields (0.5mm2 each) were blindly selected throughout the tissue and each tumor within the image field was precisely marked. To highlight the precision of this selection please see Supplementary Fig. 13b. The software then calculated for each image the number

of micro-metastastic foci and their relative tumor area [(tumor area/total tissue area)x100]. For each mouse, 2 different tissue sections were analyzed, each corresponding to a different tissue plane, sectioned ~ 500μM apart.

LDC1267 treatments in the B16F10 metastatic melanoma model

At day 0, 8-12 weeks old syngeneic C57BL/6J wild type mice were challenged with $2.5x10^5$ B16F10 cells (i.v.). The daily treatment with LDC1267 (20mg/kg, i.p.) started 24 hours later (day +1) and continued every 12 hours, until the experimental endpoint at day +14. Control mice were treated with vehicle only (90% PEG400:10% DMSO). For studying the role of NK cells, anti-NK.1.1 Abs (clone PK136) were used following the immunodepletion protocol described above. Mice were euthanized at day +14 to quantify lung melanoma metastases using the Definiens analyzer Software. At the time of dissection a careful examination of all internal organs was performed to determine the presence of extrapulmonary metastases.

Warfarin studies

Gas6 inhibition *in vivo* was performed as previously described22. Briefly, mice were treated in their drinking water with 0.5mg/l warfarin (Coumadin®, Bristol-Myers Squibb) dissolved in an ethanol/glycerol solution. Control mice were treated with the ethanol/glycerol vehicle solution only. Solutions were prepared fresh every 3-4 days. The treatment started at day -5 before tumor inoculation and continued until the endpoint of the experiment. Warfarin- and vehicle-treated mice were intravenously injected with B16F10 tumor cells as described above. To determine the role of NK cells in warfarin anti-metastatic activity, vehicle- and warfarin-treated mice were either left untreated or depleted of NK cells by administration of anti-NK1.1 depleting antibodies. At day +16, mice were euthanized and melanoma metastases to the lung and extra-pulmonary organs quantified. Prothrombine time was measured on plasma samples collected from warfarin-treated and vehicle-treated mice at the experimental endpoint (day +16) using an Amelung KC coagulometer (performed by In Vitro-Labor GmbH, Vienna, Austria). Warfarin effects on NK cytotoxicity were also evaluated by intraperitoneal injection of a mixture of NK cell resistant and sensitive cells (RMA:RMA-S or RMA:RMA-Rae1) into warfarin and vehicle-treated mice as described above.

Statistical analyses

Unless otherwise stated data are shown as mean values ± standard error of the mean (s.e.m). The numbers of mice per group used in each experiment are annotated in the corresponding figure legends as n. All experiments shown were reproduced 2-5 independent times. Figures and statistical analyses were generated using GraphPad Prism 5 (GraphPad Software Inc.). For tumor experiments, only mice that developed tumors were included in the analysis and all tumor quantifications were performed blindly by using the Definiers Software analyzer. Mice were allocated to experimental groups based on their genotype and randomized within the given sex- and age- matched group. Given that our mice were inbred and matched for age and sex, we always assumed similar variance between the different experimental groups. We did not performed an a priori sample size estimation but always used as many mice per group as possible in an attempt to minimize type I and type II errors. Critical experiments

Europe PMC Funders Author Manuscripts

have high n numbers and were repeated multiple times. Data was first analyzed for normal distribution using D'Agostino and Pearson omnibus normality tests. Normally distributed data was analyzed using unpaired two-tailed Student's t-test for single comparisons, and one-way or two-way analysis of variance –ANOVA- for multiple comparisons. ANOVA analyses were followed by Dunnett's, Bonferroni's or Tukey's post hoc tests. Ordinal and not normally distributed data was analyzed using unpaired two-tailed Mann-Whitney test for single comparisons or Kruskal-Wallis test followed by Dunn's post hoc test for multiple comparisons. The prevalence of secondary metastases was analyzed using the Chi-square test. Overall survival to tumor challenge was analyzed in Kaplan-Meier curves using a log-rank test. The statistical test used and p values are indicated in each figure legend. $p \leq 0.05$ was considered to indicate statistical significance. *P ≤0.05, **P ≤0.01, ***P ≤0.001. n.s., not significant.

Europe PMC Funders Author Manuscripts

Extended Data

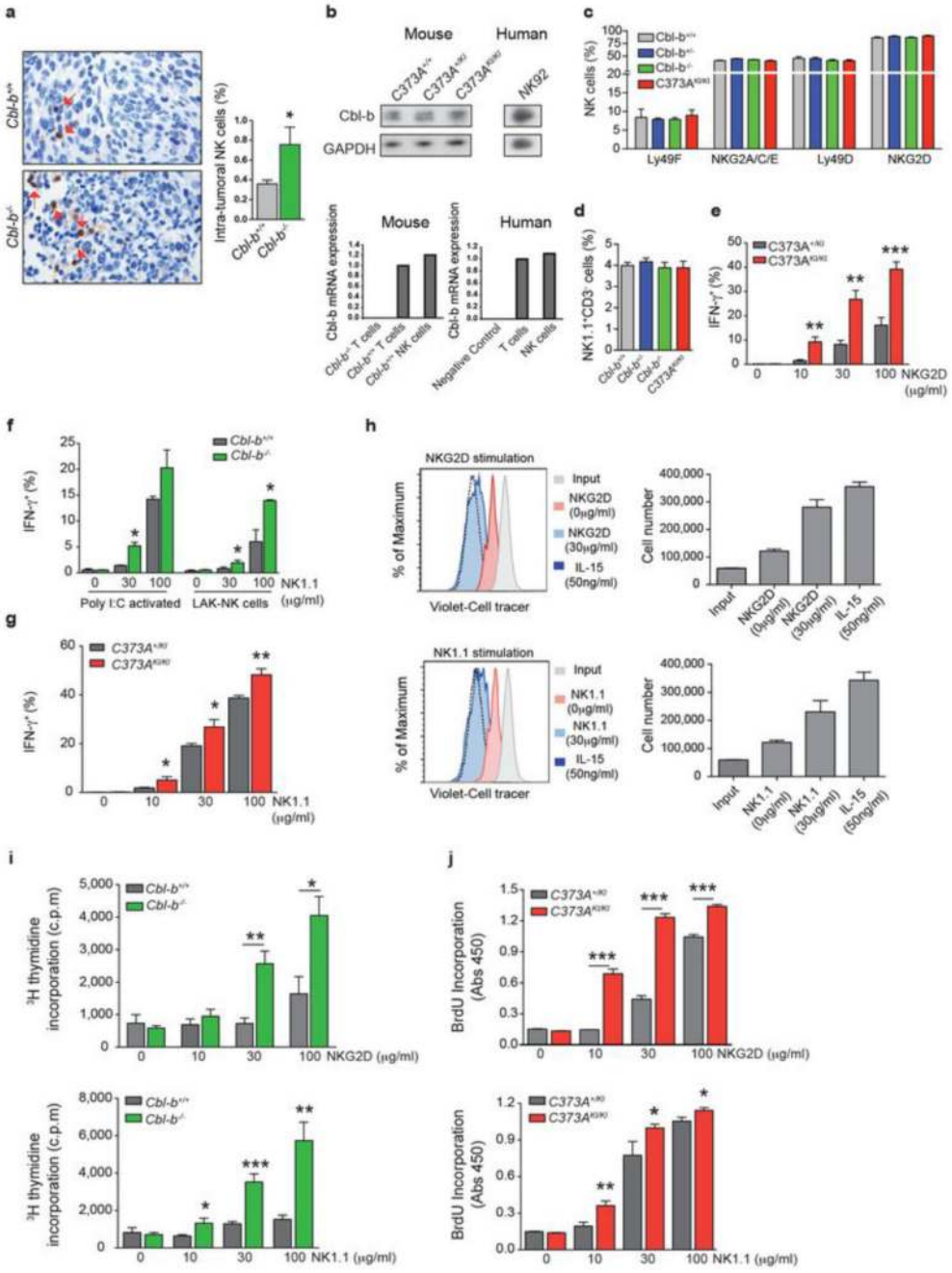

Extended Data Figure 1. Cbl-b mutant NK cells are hyper-reactive.

a, Immunohistochemistry for NKp46 to detect NK cells in tumors isolated from *Cbl-b*$^{+/+}$ and *Cbl-b*$^{-/-}$ mice at post TC-1 inoculation day 14, when all experimental mice had similar tumor volumes (left). Tumor infiltrating NK cells (%) in *Cbl-b*$^{+/+}$ and *Cbl-b*$^{-/-}$ mice as detected by NKp46 immunohistochemistry (right). (mean ± s.e.m, n=4 each). *P<0.05 (Student's t-test). **b,** Western blot for Cbl-b and GAPDH in FACS sorted *C373A*$^{+/+}$, *C373A*

+/KI, and *C373A$^{KI/KI}$* murine NK cells and the human NK cell line NK92 (upper panel). Quantitative Cbl-b mRNA expression in sorted primary wild-type murine and human NK and T cells (bottom panels). *Cbl-b$^{-/-}$* T cells and H_20 samples were used as negative controls. **c**, Ly49D, Ly49F, NKG2A/C/E, and NKG2D expressing NK cells (%), as determined by FACS (mean ± s.e.m, n=5-8). Gated on NK1.1$^+$CD3ε$^-$ or Dx5$^+$CD3ε$^-$ NK cells. **d,** Percentage of splenic NK1.1$^+$CD3ε$^-$ cells in *Cbl-b$^{+/+}$*, *Cbl-b$^{+/-}$*, *Cbl-b$^{-/-}$*, and *C373A$^{KI/KI}$* mice as determined by FACS. (mean ± s.e.m., n=5-8). No significant differences were observed among any of the NK cell subpopulations analyzed in **c** and **d** (One-way ANOVA). **e,** Percentage of IFN-γ producing *C373A$^{+/KI}$* and *C373A$^{KI/KI}$* NK cells upon stimulation with anti-NKG2D Abs. (mean ± s.e.m., n=3, representative of 4). **P<0.01, ***P<0.001 (Student's t-test). **f-g,** IFN-γ producing NK cells (%) upon NK1.1 stimulation of primary NK cells isolated from *Cbl-b$^{+/+}$* and *Cbl-b$^{-/-}$* poly I:C-treated mice **(f)**, and *ex vivo* expanded (LAK) *Cbl-b$^{+/+}$* and *Cbl-b$^{-/-}$* **(f)**, as well as *C373A$^{+/KI}$* and *C373A$^{KI/KI}$* **(g)** NK cells. (mean ± s.e.m., n=3, representative of 3.). *P<0.05, **P<0.01 (Student's t-test). **h,** *In vitro* proliferation studies on wild-type *ex vivo* expanded NK cells treated with anti-NK1.1 or anti-NKG2D antibodies as determined by cell tracer FACS analysis (left) and absolute cell number quantification (right). IL-15 stimulation was used as positive control. **i-j,** *In vitro* proliferation of *Cbl-b$^{+/+}$* and *Cbl-b$^{-/-}$* (**i**), and *C373A$^{+/KI}$* and *C373A$^{KI/KI}$* (**j**) NK cells treated with the indicated concentrations of plate-bounded anti-NK1.1 and NKG2D antibodies. (mean ± s.e.m., n=3, representative of at least 3). *P<0.05, **P<0.01, ***P<0.001 (Student's t-test).

Europe PMC Funders Author Manuscripts

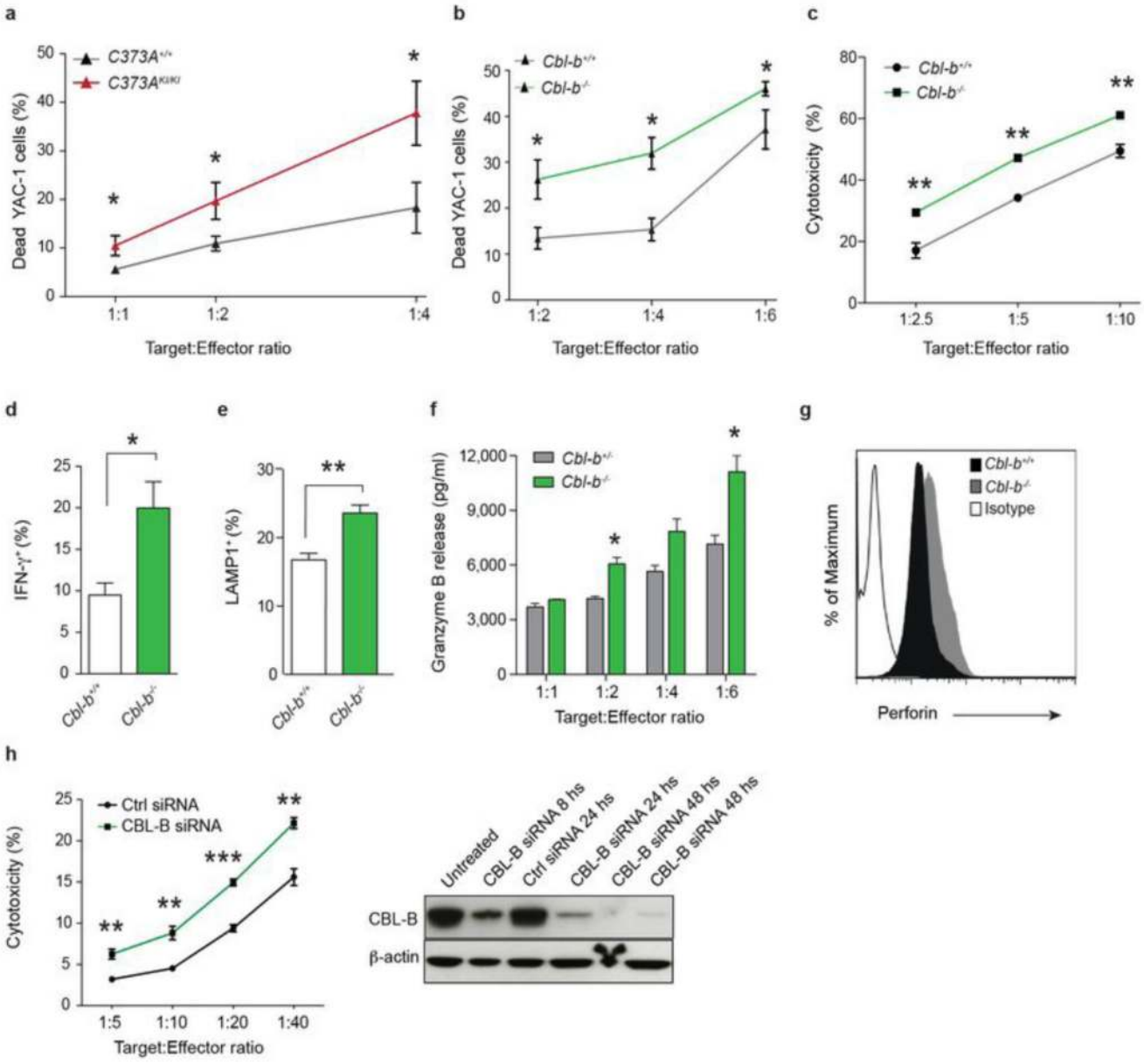

Extended Data Figure 2. Cbl-b controls NK cell cytotoxicity.

a-c, *In vitro* NK cell cytotoxicity of *C373A*$^{+/+}$ and *C373A*$^{KI/KI}$ (**a**) and *Cbl-b*$^{+/+}$ and *Cbl-b*$^{-/-}$ NK cells (**b-c**) towards YAC-1 targets as quantified by FACS analysis of TO-PRO-3 iodide^{+} YAC-1 cells (**a-b**) and ^{51}Cr-release assay (**c**). (mean values ± s.e.m., n=3). *P<0.05, **P<0.01, and ***P<0.001 (Student's t-test). **d,** Percentages of IFN-γ producing *Cbl-b*$^{+/+}$ and *Cbl-b*$^{-/-}$ NK cells upon incubation with YAC-1 targets (effector:target ratio 2:1, 6 hours). (mean ± s.e.m., n=3). *P<0.05 (Student's t-test). **e,** Degranulating murine NK cells (%) upon co-culture with YAC-1 targets, as determined by surface exposure of LAMP-1 (mean ± s.e.m., n=3). **P<0.01 (Student's t-test). **f,** Granzyme B release in the supernatant NK cells:YAC-1 co-cultures, at different effector:target ratios. (mean ± s.e.m., n=3). *P<0.05 (Student's t-test). **g,** Histogram for perforin expression in murine *Cbl-b*$^{+/+}$ and *Cbl-b*$^{-/-}$ NK

cells upon incubation with YAC-1 cells (effector:target ratio 2:1). **h**, Cytotoxic activity of scrambled control-siRNA and Cbl-b siRNA treated human NKL cells towards Jurkat cells at different effector:target ratios 48 hours after siRNA transfection. Western blot verifying Cbl-b knockdown efficiency 8, 24, and 48 hours after transfection is shown (left panel). **P<0.01, ***P<0.001 (Student's t-test). For **a-g** *ex vivo* expanded (LAK) NK cells were used. Data is representative of at least 2 independent experiments.

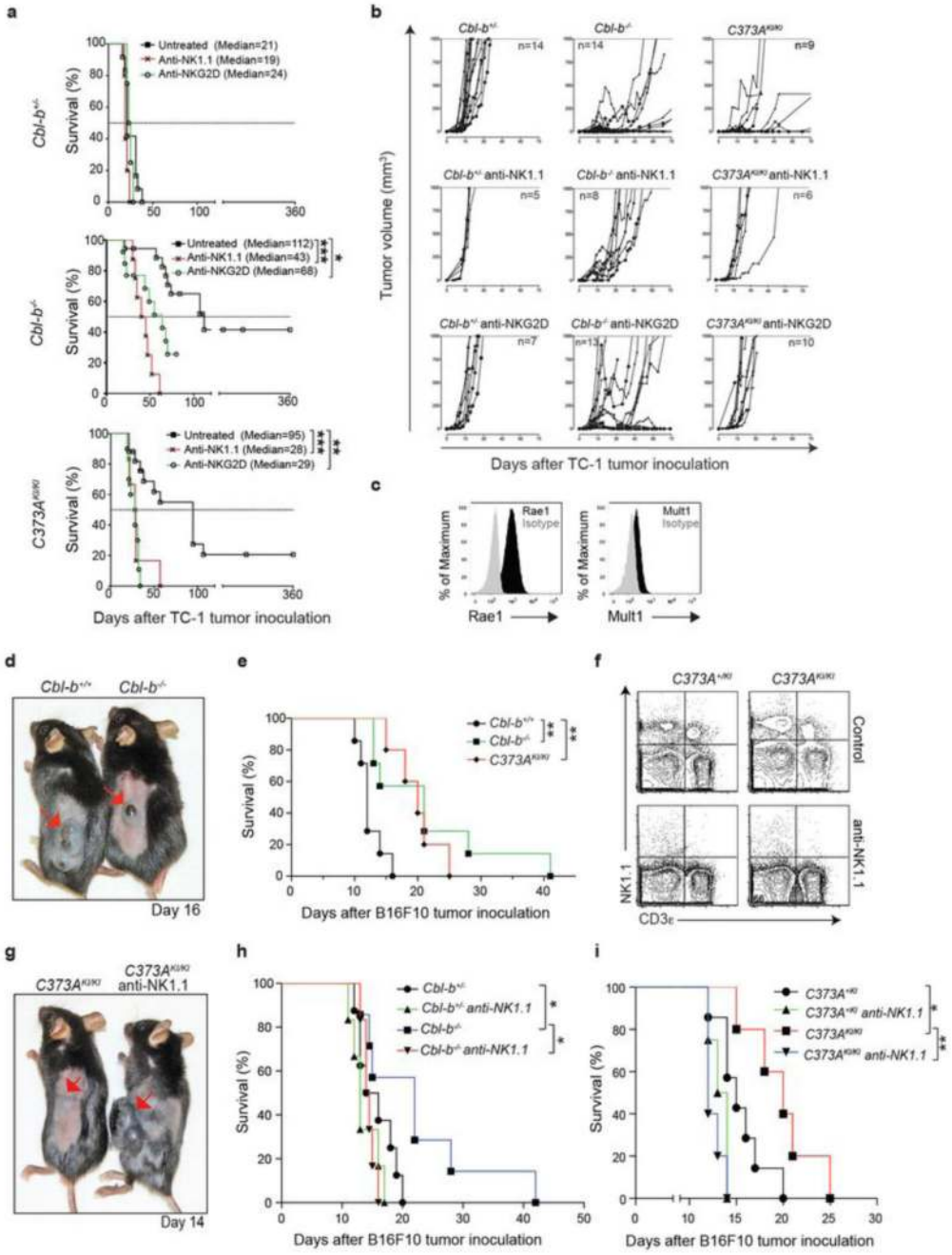

Extended Data Figure 3. Cbl-b, acting as an E3 ligase, controls NK cell mediated rejection of subcutaneous TC-1 tumors and melanomas.

Europe PMC Funders Author Manuscripts

a, Overall survival rates of untreated, NK1.1^{+}-depleted, and NKG2D-blocked *Cbl-b*$^{+/-}$, *Cbl-b*$^{-/-}$ and *C373A*$^{KI/KI}$ mice challenged with subcutaneous TC-1 tumors. Median survival values are shown (n=5-14). *P<0.05, **P<0.01, ***P<0.001 (log-rank test). No significant difference was found between the untreated and treated *Cbl-b*$^{+/-}$ groups. **b,** Kinetics of TC-1 tumor cell growth in individual control (upper panels), NK1.1-depleted (middle panels) and NKG2D-blocked (bottom panels) *Cbl-b*$^{+/+}$, *Cbl-b*$^{-/-}$, and *C373A*$^{KI/KI}$ mice. The numbers of experimental mice are indicated for each experiment and genotype (n). **c,** Histograms showing the expression of the NKG2D ligands Rae1 and Mult1 on TC-1 tumor cells (black). Isotype controls are shown in grey. **d,** Representative photographs showing B16F10 subcutaneous tumors in *Cbl-b*$^{+/+}$ and *Cbl-b*$^{-/-}$ mice at day +16 post-tumor s.c. inoculation. **e,** Overall survival for *Cbl-b*$^{+/+}$, *Cbl-b*$^{-/-}$, and *C373A*$^{KI/KI}$ mice subcutaneously challenged with 2.5x10^{5} B16F10 melanoma cells (n=5-7). **P<0.001 *Cbl-b*$^{-/-}$ or *C373A*$^{KI/KI}$ vs. *Cbl-b*$^{+/+}$ mice (log-rank test). **f,** Representative FACS blots for NK1.1^{+} and CD3ε^{+} cell populations in *C373A*$^{+/KI}$ and *C373A*$^{KI/KI}$ littermate mice, confirming efficient splenic NK1.1^{+} cell depletion in mice receiving anti-NK1.1 antibodies. **g,** Representative images of untreated *C373A*$^{KI/KI}$ and NK1.1-depleted *C373A*$^{KI/KI}$ tumor-bearing mice at day +14 post-B16F10 inoculation. **h,** Overall survival of untreated and NK1.1-depleted *Cbl-b*$^{+/-}$ and *Cbl-b*$^{-/-}$ littermates subcutaneously challenged with 2.5x10^{5} B16F10 cells (n=6-8). *P<0.05 *Cbl-b*$^{-/-}$ vs *Cbl-b*$^{+/-}$ and NK1.1-depleted *Cbl-b*$^{-/-}$ groups (log-rank test). **i,** Overall survival of untreated and NK1.1-depleted *C373A*$^{+/KI}$ and *C373A*$^{KI/KI}$ mice subcutaneously challenged with 2.5x10^{5} B16F10 cells (n=4-7). *P<0.05 *C373A*$^{+/KI}$ vs *C373A*$^{KI/KI}$, **P<0.01 *C373A*$^{KI/KI}$ vs NK1.1-depleted *C373A*$^{KI/KI}$ (log-rank test).

Europe PMC Funders Author Manuscripts

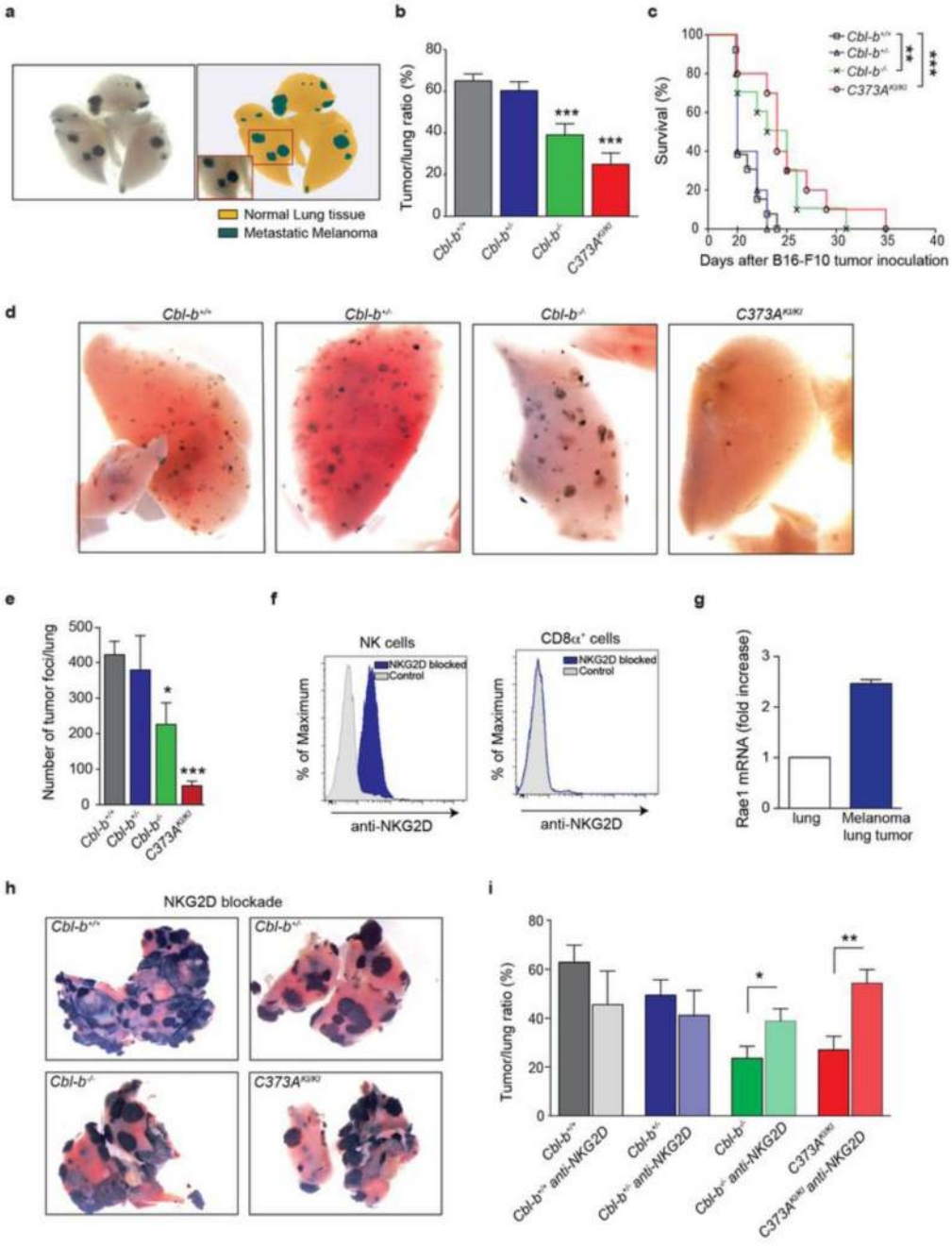

Extended Data Figure 4. Cbl-b mutant NK cells can efficiently control melanoma lung metastases.

a, Automated quantification of lung and melanoma tumor areas using the Definiens Tissue software. An algorithm was developed to identify and categorize the lung images into normal lung tissue (yellow) and metastatic melanoma (green). The higher magnification inset in the lower panel highlights the precision of the quantification. **b**, Tumor-to-lung ratios (%) in *Cbl-b*$^{+/+}$(n=14), *Cbl-b*$^{+/-}$ (n=9), *Cbl-b*$^{-/-}$ (n=11) and *C373A*$^{KI/KI}$ (n=11) mice 21 days after intravenous injection of 2.5x10^{5}B16F10 melanoma cells (mean ± s.e.m.). ***P<0.001

Europe PMC Funders Author Manuscripts

Cbl-b$^{+/+}$ vs *Cbl-b*$^{-/-}$ and *C373A*$^{KI/KI}$ groups (One-way ANOVA, Dunnett's post hoc test). **c,** Overall survival of *Cbl-b*$^{+/+}$ (n=13), *Cbl-b*$^{+/-}$ (n=5), *Cbl-b*$^{-/-}$ (n=10), and *C373A*$^{KI/KI}$ (n=10) mice i.v. challenged with 2.5x10^5 B16F10 cells. **P<0.01 *Cbl-b*$^{-/-}$ vs. *Cbl-b*$^{+/+}$ groups. ***P<0.001 *C373A*$^{KI/KI}$ vs. *Cbl-b*$^{+/+}$ groups (log-rank test). **d,** Representative lung photographs in *Cbl-b*$^{+/+}$, *Cbl-b*$^{+/-}$, *Cbl-b*$^{-/-}$, and *C373A*$^{KI/KI}$ mice 7 days after i.v. inoculation with 7.5x10^5 B16F10 cells. **e,** Quantification of total numbers of tumor foci in the lungs of Cbl-b$^{+/+}$, *Cbl-b*$^{+/-}$, *Cbl-b*$^{-/-}$, and *C373A*$^{KI/KI}$ mice treated as described in **d** (mean ± s.e.m., n=5-6). *P<0.05 *Cbl-b*$^{-/-}$ vs *Cbl-b*$^{+/+}$ and ***P<0.001 *C373A*$^{KI/KI}$ vs. *Cbl-b*$^{+/+}$ mice (Student's t-test). **f,** Histograms showing binding of the anti-NKG2D blocking antibodies to splenic NK cells in NKG2D-blocked *Cbl-b*$^{-/-}$ mice at the day of tumor inoculation (day 0). Anti-NKG2D antibodies were detected using anti-rat secondary Abs. Histograms are gated on NK (NK1.1$^+$CD3ε$^-$) and CD8$^+$ T cells (CD3ε$^+$CD8α$^+$). Note that in this naïve unchallenged mice, the blocking antibodies do not bind to CD8$^+$ T cells. Untreated *Cbl-b*$^{-/-}$ mice are shown as controls**. g,** Quantitative PCR showing Rae1 mRNA expression in B16F10 melanoma tumors isolated from the lung of tumor bearing mice (day +16 after tumor challenge). Data is relative to the expression levels of Rae1 mRNA in healthy lung tumors isolated from non-tumor bearing mice. **h,** Photographs of individual lungs of *Cbl-b*$^{+/+}$, *Cbl-b*$^{+/-}$, *Cbl-b*$^{-/-}$, and *C373A*$^{KI/KI}$ mice treated with the anti-NKG2D blocking Abs and i.v. challenged with B16F10. Images are from day +21. Photographs for untreated mice are shown in Fig. 1e. **i,** Tumor-to-lung ratios (%) of control and anti-NKG2D-blocked *Cbl-b*$^{+/+}$, *Cbl-b*$^{+/-}$, *Cbl-b*$^{-/-}$, and *C373A*$^{KI/KI}$ mice 21 days after B16F10 tumor-inoculation (mean ± s.e.m., n=5-12). *P<0.05 *Cbl-b*$^{-/-}$ vs. *Cbl-b*$^{-/-}$ NKG2D-blocked mice; **P<0.01 *C373A*$^{KI/KI}$ vs. NKG2D-blocked *C373A*$^{KI/KI}$ mice (Student's t-test).

Europe PMC Funders Author Manuscripts

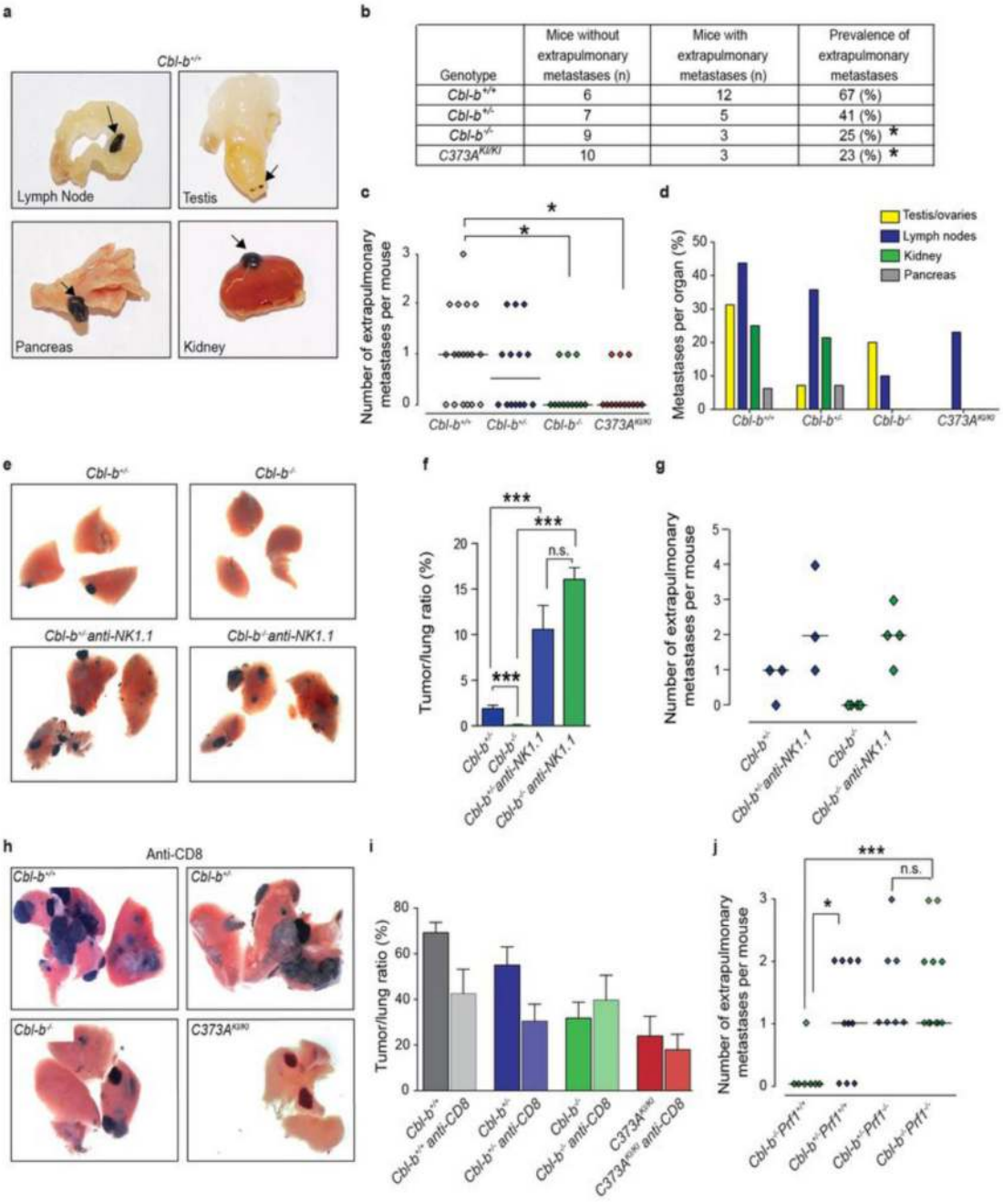

Genotype	Mice without extrapulmonary metastases (n)	Mice with extrapulmonary metastases (n)	Prevalence of extrapulmonary metastases
Cbl-b$^{+/+}$	6	12	67 (%)
Cbl-b$^{+/-}$	7	5	41 (%)
Cbl-b$^{-/-}$	9	3	25 (%) *
C373A$^{KI/KI}$	10	3	23 (%) *

Extended Data Figure 5. The role CD8^{+} cells and perforin-mediated cytotoxicity in controlling melanoma mestastasis.

a, Photographs of melanoma metastases found in the pancreas, kidney, testis, and lymph node of *Cbl-b*$^{+/+}$ mice 21 days post-tumor inoculation. Similar results were observed in *Cbl-b*$^{+/-}$ mice. **b,** Prevalence of extrapulmonary melanoma metastases in *Cbl-b*$^{+/+}$, *Cbl-b*$^{+/-}$, *Cbl-b*$^{-/-}$, and *C373A*^{KIKI} mice, defined by the presence of macroscopically visible melanoma tumors in any organ other than the lung, regardless of the number of organs affected per mouse. Data are from day +21 post-tumor challenge. *P<0.05 *Cbl-b*$^{-/-}$ and *C373A*^{KIKI} vs.

Cbl-b$^{+/+}$ groups (Chi-square test). **c,** Numbers of extra-pulmonary metastases per mouse in *Cbl-b*$^{+/+}$, *Cbl-b*$^{+/-}$, *Cbl-b*$^{-/-}$, and *C373A*$^{KI/KI}$ mice (day +21). Data from individual mice (n=12-18) and median values are shown (horizontal lines). *P<0.05 *Cbl-b*$^{-/-}$ or *C373A*$^{KI/KI}$ vs. *Cbl-b*$^{+/+}$ group (Mann-Whitney test). **d,** Presence of melanoma metastases (%) in different tissues of *Cbl-b*$^{+/+}$ (n=16), *Cbl-b*$^{+/-}$ (n=10), *Cbl-b*$^{-/-}$ (n=9), and *C373A*$^{KI/KI}$ (n=11) mice (day +21). **e,** Representative lung photographs of untreated and NK1.1^{+} cell-depleted *Cbl-b*$^{+/-}$ and *Cbl-b*$^{-/-}$ mice 28 days after i.v. injection of a 10 times lower dose of B16F10 tumor cells (2.5x10^{4}). **f,** Tumor-to-lung ratios (%) of non-depleted and NK1.1^{+}-depleted *Cbl-b*$^{+/-}$ and *Cbl-b*$^{-/-}$ mice treated as described in **e**. Data are mean values ± s.e.m. at the experimental endpoint. (n=3-4). ***P<0.001, n.s.=not significant (Student's t-test). **g, Number of** extrapulmonary tumor metastases in control or NK1.1-depleted *Cbl-b*$^{+/-}$ and *Cbl-b*$^{-/-}$ mice 28 days after injection of 2.5x10^{4} B16F10 tumor cells. Horizontal lines are median values. **h**, Representative lung photographs of CD8^{+} cell-depleted *Cbl-b*$^{+/+}$, *Cbl-b*$^{+/-}$, *Cbl-b*$^{-/-}$ and *C373A*$^{KI/KI}$ mice 21 days after i.v. injection of B16F10 tumor cells. **i**, Tumor-to-lung ratios (%) of non-depleted *Cbl-b*$^{+/+}$ (n=12), *Cbl-b*$^{+/-}$ (n=6), *Cbl-b*$^{-/-}$ (n=9), and *C373A*$^{KI/KI}$ (n=7) and CD8^{+}-depleted *Cbl-b*$^{+/+}$(n=6), *Cbl-b*$^{+/-}$ (n=4), *Cbl-b*$^{-/-}$ (n=4), and *C373A*$^{KI/KI}$ (n=4) mice. Data are mean values ± s.e.m. at the experimental endpoint. Of note, we observed a reduction in the tumor/lung ratios of *Cbl-b*$^{+/+}$ and *Cbl-b*$^{+/-}$ mice following *in vivo* depletion of CD8^{+} cells, a finding that requires further explorations. **j**, Numbers of extrapulmonary melanoma metastases in *Cbl-b*$^{+/-}$ *Prf1*$^{+/+}$ (n=10), *Cbl-b*$^{-/-}$ *Prf1*$^{+/+}$ (n=7), *Cbl-b*$^{+/-}$ *Prf1*$^{-/-}$ (n=7) and *Cbl-b*$^{-/-}$ *Prf1*$^{-/-}$ (n=11) mice at the experimental endpoint (day +21). *P<0.05, **P<0.01 (Mann-Whitney test).

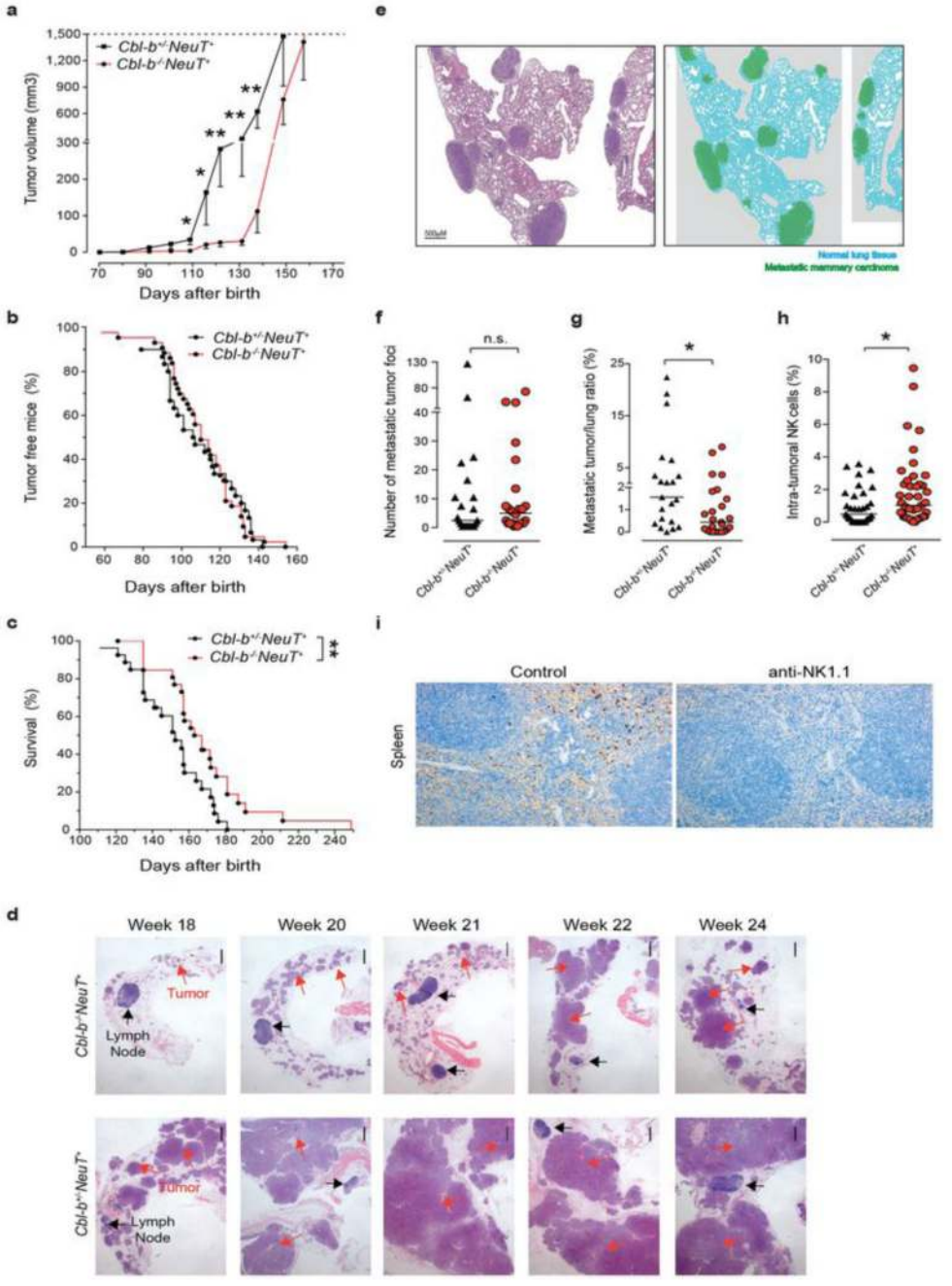

Extended Data Figure 6. Mice deficient in Cbl-b can control the growth of NeuT^{+} mammary and metastatic lung tumors.

a, Kinetics of NeuT^{+} mammary tumor growth in *Cbl-b$^{+/-}$NeuT^{+}* and *Cbl-b$^{-/-}$NeuT^{+}* mice (n=27 for each). Data are mean values ± s.e.m. *P<0.05, **P<0.01 (Student's t-test). **b,** Onset of palpable mammary tumors in *Cbl-b$^{+/-}$NeuT^{+}* (n=30) and *Cbl-b$^{-/-}$NeuT^{+}* (n=43) transgenic mice. The median tumor onset for *Cbl-b$^{+/-}$NeuT^{+}* and *Cbl-b$^{-/-}$NeuT^{+}* mice was 107 and 110 days after birth, respectively. P>0.05, not significant (log-rank test). **c,** Overall survival for *Cbl-b$^{+/-}$NeuT^{+}* and *Cbl-b$^{-/-}$NeuT^{+}* mice (n=27 for each). Mice were euthanized

Europe PMC Funders Author Manuscripts

when total tumor volume of all affected mammary glands reached 1500mm^3. **P<0.01 (log-rank test). **d,** Histological appearance of isolated mammary glands in 18, 20, 21, 22, and 24 weeks old *Cbl-b*$^{+/-}$*NeuT*$^+$ and *Cbl-b*$^{-/-}$*NeuT*$^+$ littermates. Red arrows indicate mammary tumors, black arrows the axillary lymph nodes. H&E staining. Bars, 1mm. **e,** Representative images for the automated quantification of metastatic lung mammary carcinomas in mice bearing NeuT$^+$ mammary tumors using a customized algorithm in Definiens Tissue Software to identify and categorize 2 areas: normal lung tissue (blue), and metastatic mammary carcinoma (green). **f,g,** Numbers of tumor foci (**f**) and tumor-to-lung area (%) (**g**) in lungs of *Cbl-b*$^{+/-}$*NeuT*$^+$ and *Cbl-b*$^{-/-}$*NeuT*$^+$ mice bearing NeuT$^+$ mammary tumors (n=17/20). At least 2 lung images were quantified per mouse (≥350μm apart). *P<0.05 (Mann-Whitney test, lines are median values). **h,** Quantification of NK cells infiltrating the metastatic mammary lung carcinomas of *Cbl-b*$^{+/-}$*NeuT*$^+$ and *Cbl-b*$^{-/-}$*NeuT*$^+$ mice, as detected by immunohistochemistry for NKp46 and quantified using the Definiens Software (n=13-15 per genotype, line are median). *P<0.001 (Mann-Whitney test). **i,** Images showing specific staining of NK cells in spleen using the anti-NKp46 antibody. Untreated and NK-cell depleted animals were used as positive and negative controls respectively.

Europe PMC Funders Author Manuscripts

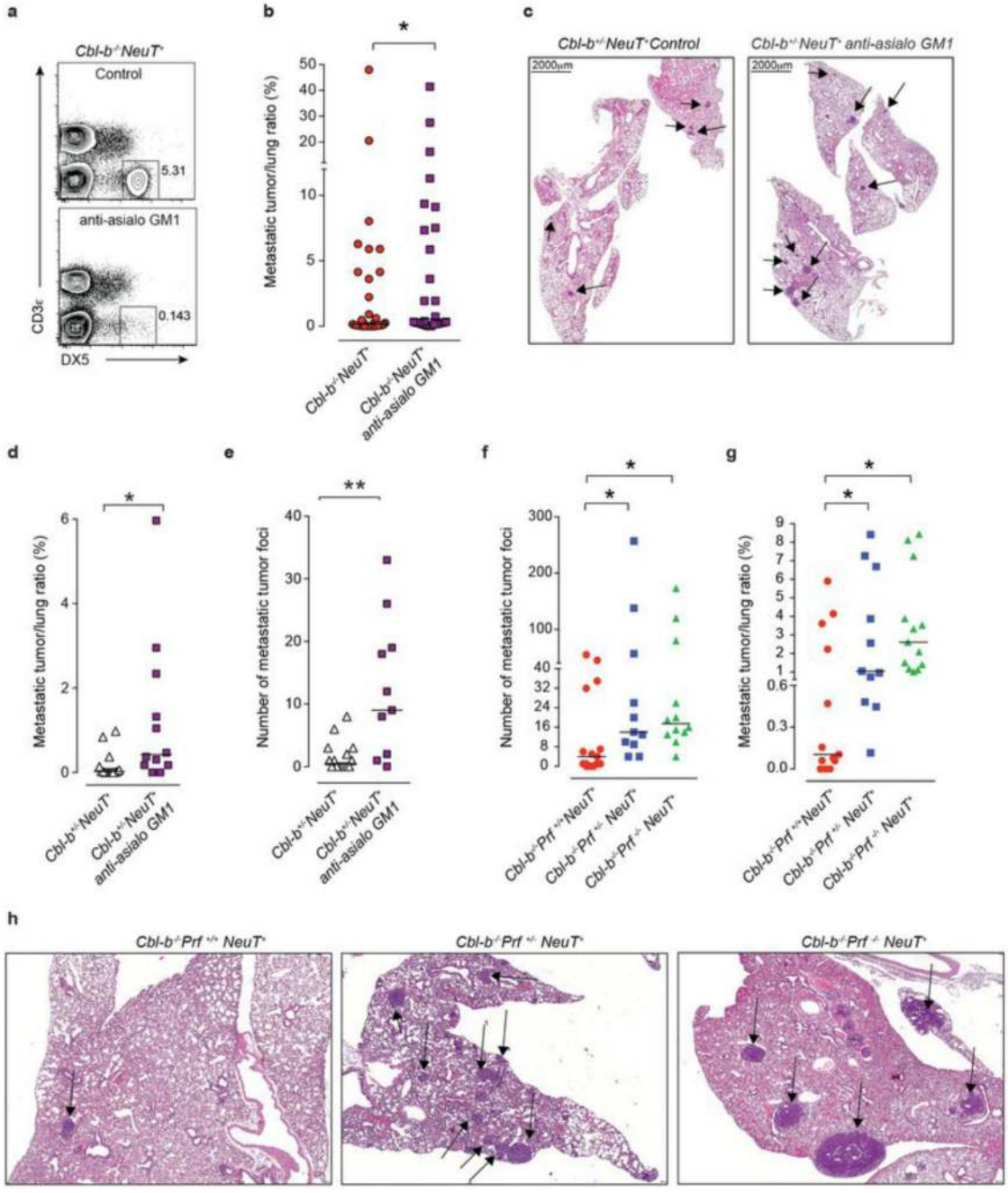

Extended Data Figure 7. Cytotoxic NK cells are required for the efficient control of mammary cancer metastases to the lung.

a, Flow cytometry blots for DX5$^+$ and CD3ε$^+$ cell populations in untreated and anti-asialo GM1-treated *Cbl-b*$^{-/-}$*NeuT*$^+$ mice confirming efficient splenic NK cell depletion at the experimental endpoint. Numbers indicate percentages of DX5$^+$ NK cells in the respective gates. **b,** Tumor-to-lung area (%) for metastatic mammary carcinoma in the lungs of control and anti-asialo GM1-treated *Cbl-b*$^{-/-}$*NeuT*$^+$ mice (n=11/10). Median values are shown with a horizontal line. *P<0.05 (Mann-Whitney test). **c,** Representative H&E-stained lung sections

Europe PMC Funders Author Manuscripts

of control and anti-asialo GM1-treated *Cbl-b*$^{+/-}$*NeuT*$^{+}$ mice showing metastatic mammary carcinomas (arrows). **d-e,** Relative tumor-to-lung areas (%) (**d**) and numbers of metastatic tumor foci **(e)** in the lungs of control and anti-asialo GM1-treated *Cbl-b*$^{+/-}$*NeuT*$^{+}$ mice (n=6-7, 2 sections per mouse were quantified). *P<0.05 **P<0.01 (Mann-Whitney test). Lines are median values. **f-g,** Numbers of tumor foci **(f)** and relative tumor-to-lung area (%) **(g)** in the lungs of *Cbl-b*$^{-/-}$*Prf1*$^{+/+}$*NeuT*$^{+}$, *Cbl-b*$^{-/-}$*Prf1*$^{+/-}$*NeuT*$^{+}$, and *Cbl-b*$^{-/-}$*Prf1*$^{-/-}$*NeuT*$^{+}$ mice (n=5-6, lines are median values. At least 2 sections per mouse were quantified. *P<0.05 (Mann-Whitney test). **h,** Representative H&E-stained lung sections of *Cbl-b*$^{-/-}$*Prf1*$^{+/+}$*NeuT*$^{+}$, *Cbl-b*$^{-/-}$*Prf1*$^{+/-}$*NeuT*$^{+}$, and *Cbl-b*$^{-/-}$*Prf1*$^{-/-}$*NeuT*$^{+}$ mice showing metastatic mammary carcinomas (arrows). Note the increase in metastatic tumor foci and total tumor area even in the absence of one copy of the *perforin* gene.

Europe PMC Funders Author Manuscripts

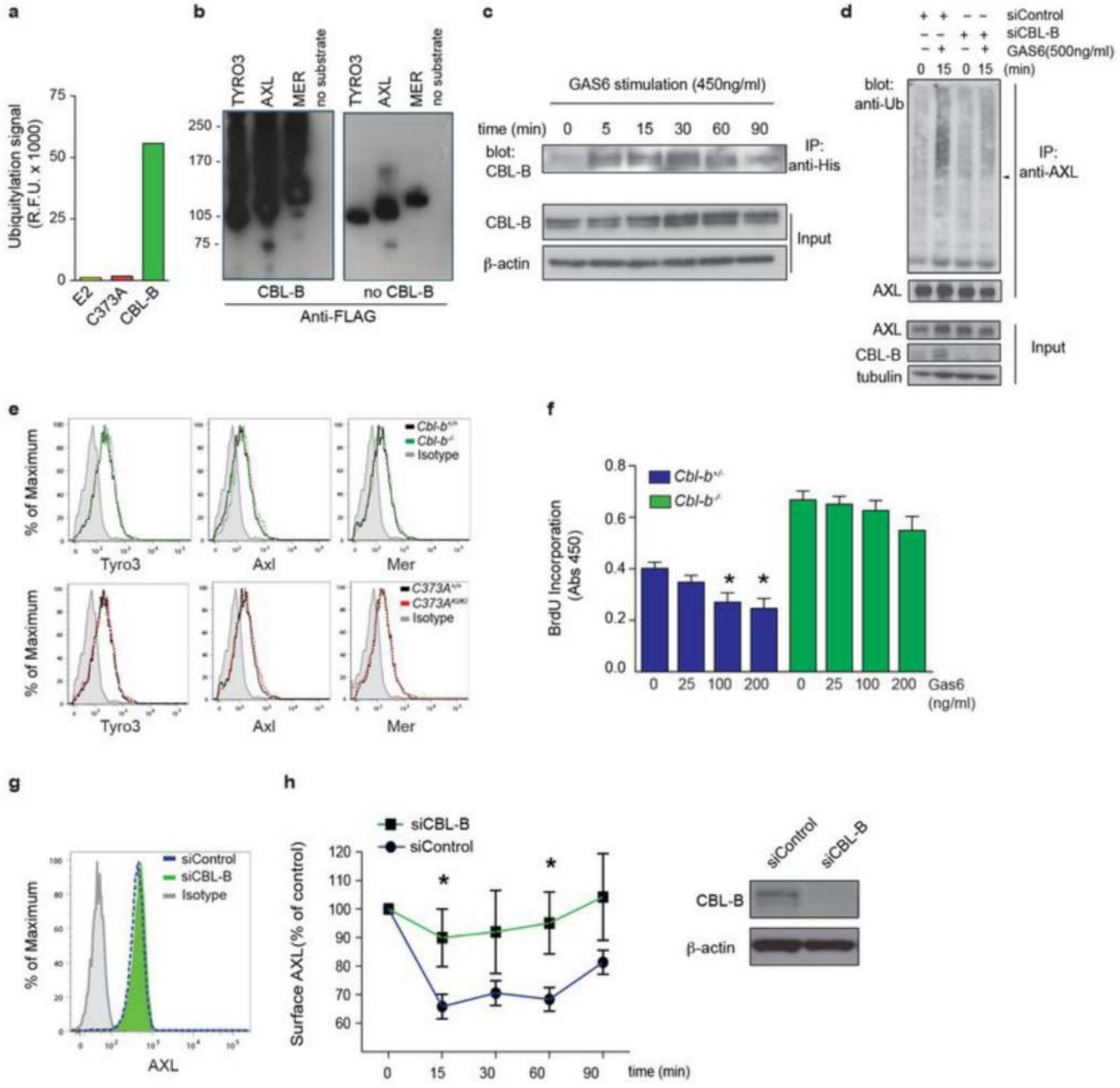

Extended Data Figure 8. TAM tyrosine kinase receptors are novel ubiquitylation targets of Cbl-b.

a, Out of 9000 human proteins tested, Tyro3 had the highest Cbl-b mediated ubiquitylation signal. Signal intensities are shown for the corresponding Tyro3 spots in the protein arrays incubated with the E2 enzyme without Cbl-b, the Cbl-b C373A mutant, and wild-type Cbl-b proteins (in duplicates). Data are shown as mean values. RFU: relative fluorescent units. **b,** *In vitro* ubiquitylation of recombinant Flag-tagged Tyro3, Axl, and Mer in the presence (left panel) and absence (right panel) of Cbl-b. Blots were probed with anti-Flag Abs. **c,** Immunoprecipitation showing time-dependent recruitment of Cbl-b to TAM tyrosine kinase

Europe PMC Funders Author Manuscripts

receptors in HeLa cells upon stimulation with His-tagged Gas6 (upper panel). Input levels of Cbl-b and β-actin are shown as controls. **d**, Gas6-induced Axl ubiquitylation depends on Cbl-b expression. HeLa cells were transfected with scrambled siControl or siCbl-b and then stimulated with 450ng/ml Gas6 for 15 minutes or left untreated. Lysates were immunoprecipiated with anti-Axl antibodies. Blots were then probed using anti-Ubiquitin and anti-Axl Abs. The location of the mature form of Axl (~140kDa) is shown with an arrow. Axl, Cbl-b, and tubulin protein levels are shown to control for the input (lower panels). **e,** Representative histograms showing equal expression of Tyro3, Axl, and Mer receptors at the cell surface of freshly isolated NK1.1^{+}CD3ε^{-} splenic *Cbl-b*$^{+/+}$ *Cbl-b*$^{-/-}$ and *C373A*$^{KI/KI}$ NK cells. Background staining with control isotype Abs is shown for each blot in grey. **f,** *In vitro* proliferation of *Cbl-b*$^{+/-}$ and *Cbl-b*$^{-/-}$ NK cells stimulated with anti-NKG2D Abs (30μg/ml) in the presence of different concentrations of Gas6 (mean values ± s.e.m., n=4). *P<0.05 compared to the reference (no Gas6) value in the *Cbl-b*$^{+/-}$ group. No significant difference was detected among the *Cbl-b*$^{-/-}$ NK cells treated with different concentrations of Gas6 (One-way ANOVA, Dunnett's post hoc test). **g,** Representative histograms showing equal expression of Axl at the cell surface of HeLa cells that were transfected with scrambled siControl or siCbl-b. Data were collected 48 hours after siRNA transfection. **h**, Axl surface expression in siControl or siCbl-b HeLa cells stimulated with 200ng/ml recombinant human Gas6 for the indicated time periods. Western blots show efficient downregulation of Cbl-b protein levels in HeLa cells 48hrs after siRNA transfection (right panel). *P<0.05 (Student's t-test).

a

PROTEIN NAME	ENTREZ GENE SYMBOL	Kd [μM]
Hepatocyte growth factor receptor	c-Met	0.013
Tyrosine protein knase receptor UFO	AXL	0.019
Proto-oncogene tyrosine-protein kinase FER	FER	0.107
Dual specificity mitogen-activated protein kinase kinase	MAP2K5	0.124
Proto-oncogene tyrosine-protein kinase ABL1	ABL1	0.154
Proto-oncogene tyrosine-protein kinase Src	SRC	0.217

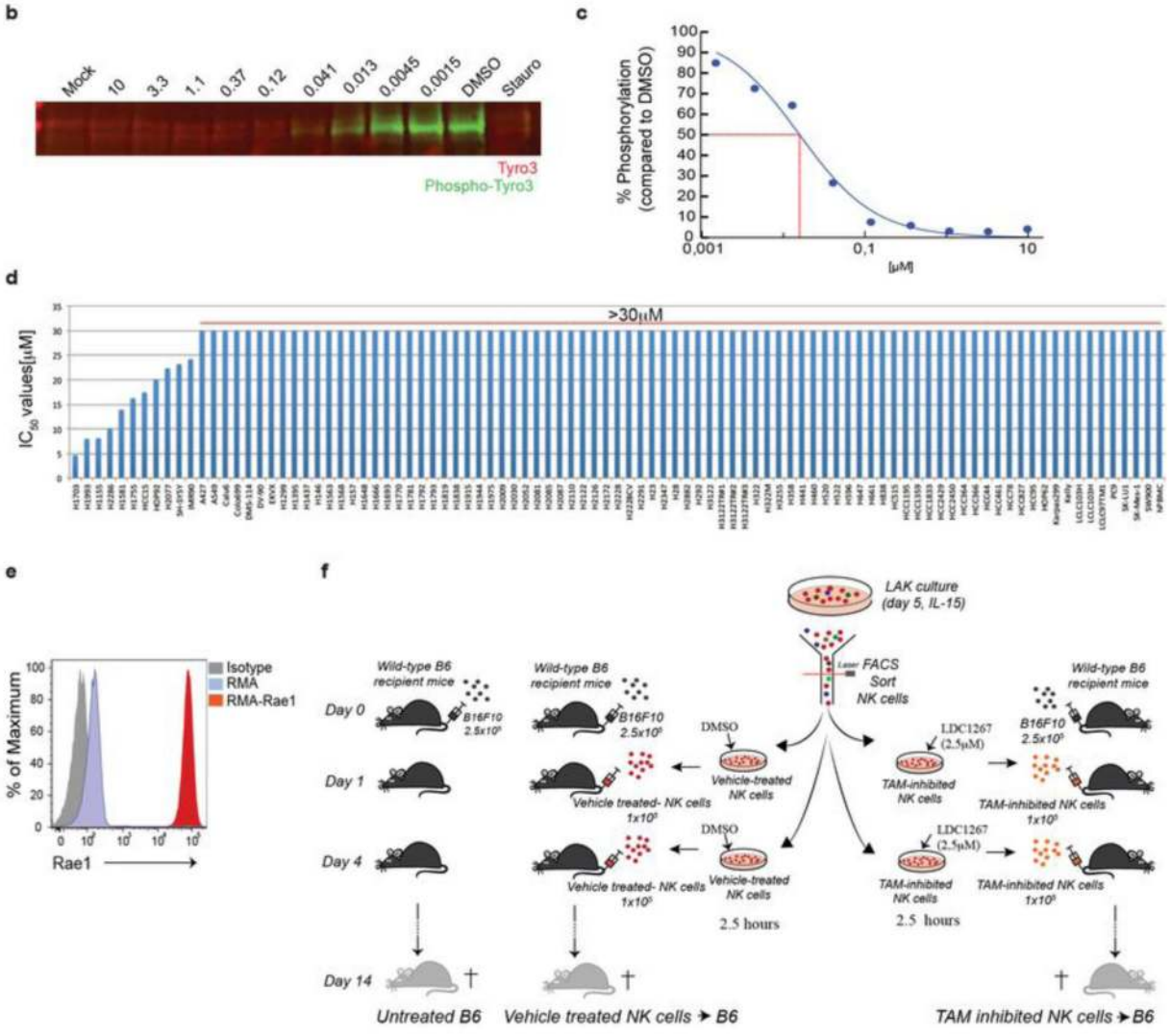

Extended Data Figure 9. Biochemical and cellular selectivity of LDC1267.

a, Target proteins of LDC1267 in Hs578T cells. Determined *K*d values are plotted on a logarithmic scale. All identified targets were protein kinases and are ranked from low (top) to high (bottom) *K*d values (in μM). The experimental procedure is summarized at http://www.evotec.com/uploads/media_library/31/2013-09_S6_Proteomics.pdf. **b-c,** Exemplary dose response curve of LDC1267 inhibition of ectopically expressed Tyro3 phosphorylation. **c,** indicates the quantification of the Western blot depicted in **b**. After transfection of HEK293 cells with Tyro3 expression plasmids cells were incubated with LDC1267 or

Europe PMC Funders Author Manuscripts

DMSO for 1hour. Protein lysates were separated by SDS-PAGE and blotted to a PVDF membrane. Tyro3 levels as well as its phosphorylation state were determined by Red/AlexaFluor680-labelled (Tyro3 expression) and green/IR800-labelled antibodies (tyrosine phosphorylation). **d,** IC50 values (Y axis in μM) of LDC1267 on a panel of 93 cancer cell lines and two primary cells (X axis; IMR90 and hPBMCs) in a proliferation assay. After incubation for 72 hours with LDC1267, CellTiterGlow reagent (Promega) was used to determine the proliferation relative to the corresponding DMSO control. **e,** Histogram confirming the high expression of the NKG2D ligand Rae1 at the cell surface of the genetically engineered RMA-Rae1 cell line. Staining with an isotype control Ab and basal expression of Rae1 in RMA cells are also shown. RMA and RMA-Rae1 cells lines were used for studying NKG2D-dependent NK cell cytotoxic responses *in vivo*. **f,** Protocol used to test the effects of LCD1267 in an NK cell adoptive transfer model for the treatment of metastatic melanoma. Wild-type C57BL/6J (B6) recipient mice were injected i.v. with $2.5x10^5$ B16F10 melanoma cells at day 0. At day +1 and +4, recipient mice received $1.0x10^5$ sorted syngeneic *Cbl-b* sufficient or *Cbl-b*$^{-/-}$ NK cells that were either pre-treated for 2.5 hours *ex vivo* with vehicle (DMSO) or LDC1267 (2.5μM). A control untreated group received tumor cells but did not receive NK cells (untreated B6). Mice were euthanized at day +14 post–tumor inoculation and lung tumor foci and total tumor areas in lungs were quantified.

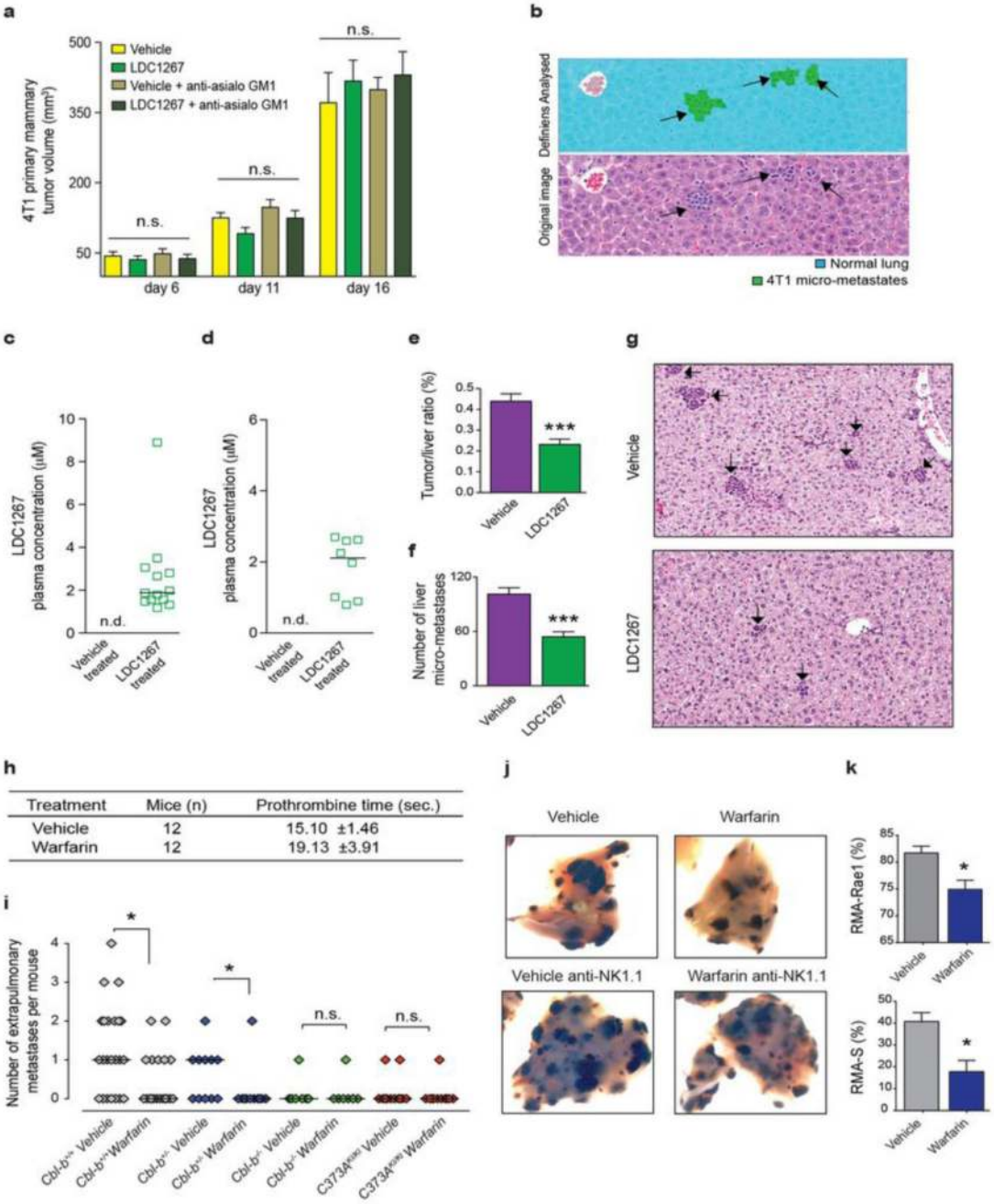

Extended Data Figure 10. Oral LDC1267 and warfarin administration reduces tumor metastases.

a, Kinetics of primary 4T1 tumor cell growth in the mammary fat pad of control and anti-asialo GM1-treated mice that received LDC1267 or vehicle (mean ± s.e.m., n=6-9 mice per group). n.s., not significant (One-Way ANOVA). **b,** Representative images for the quantification of 4T1 liver micro-metastases using the Definiens Tissue Software to identify and categorize normal lung tissue (blue) and metastatic mammary carcinoma (green, arrows). **c,** Plasma concentrations of LDC1267 in mice bearing 4T1 metastatic tumors and

Europe PMC Funders Author Manuscripts

Europe PMC Funders Author Manuscripts

treated daily by intraperitoneally injections with vehicle or LDC1267 (20mg/kg). Data is from 12 hours after the last treatment (day +16). Horizontal line indicates median value. n.d.; not detectable. **d,** Plasma concentrations of LDC1267 in mice bearing 4T1 metastatic tumors treated daily by oral gavage with vehicle or LDC1267 (100mg/kg). Data is from 11 hours after the last treatment (day +21). Horizontal line indicates median value. n.d.; not detectable. **e-f,** Relative sizes (**e**) and numbers (**f**) of 4T1 liver micro-metastases in syngeneic mice treated with vehicle or LDC1267 (100mg/kg) via oral gavage. Mean values ± s.e.m. are shown on day +21 after initiation of LDC1267 therapy (day +27 after orthotopic tumor inoculation into the mammary fat pad). ***P<0.001 (Student's t-test, n=10 mice each). **g,** Representative photographs of 4T1 liver micro-metastases in mice treated as described in **e-f**. Arrows indicate micro-metastases **h**, Prothrombine times (mean ± s.d.) in warfarin (0.5mg/l) and vehicle treated mice, showing that the low dose of warfarin used does not cause a coagulopathy, confirming previous results21,22. Of note, we never observed neither spontaneous nor excessive bleeding in warfarin-treated mice as compared to vehicle controls. Data is from mice treated orally (in drinking water) for 21 days. **i,** Numbers of extrapulmonary metastases in individual vehicle-treated *Cbl-b*$^{+/+}$ (n=23), *Cbl-b*$^{+/-}$ (n=11), *Cbl-b*$^{-/-}$ (n=7), and *C373A*$^{KI/KI}$ (n=12) and warfarin-treated *Cbl-b*$^{+/+}$ (n=19), *Cbl-b*$^{+/-}$ (n=11), *Cbl-b*$^{-/-}$ (n=9), and *C373A*$^{KI/KI}$ (n=11) mice at day +16 post B16F10 i.v. inoculation. *P<0.05 comparing the control and warfarin-treated groups in either *Cbl-b*$^{+/+}$ or *Cbl-b*$^{+/-}$ mice (Mann-Whitney test). n.s.= not significant. Horizontal lines represent median values. **j,** Representative photographs of the individual lungs of NK1.1 sufficient and NK1.1-depleted vehicle-treated and warfarin-treated *Cbl-b*$^{+/+}$ mice bearing lung metastatic melanomas. Data are from day +16 after B16F10 i.v. inoculation. **k,** *In vivo* NK cell cytotoxicity in vehicle- and warfarin-treated *Cbl-b*$^{+/+}$ mice shown as relative percentages of RMA-Rae1 and RMA-S cells cells recovered from the peritoneal cavity 24 hrs after intra-peritoneal injection of a 1:1 ratio with the NK resistant cell line RMA (mean ± s.e.m., n=5 each). Mice were treated with vehicle and warfarin for 7 days before inoculation of RMA, RMA-S and RMA-Rae1 cells. *P<0.05 (Student's t-test).

Supplementary Material

Refer to Web version on PubMed Central for supplementary material.

Acknowledgements

We thank T. Hanada, R. Hanada, R. Karim, and all other members of the Penninger laboratory for helpful discussions and technical support. We thank all members of the IMP-IMBA Biooptics service facility for assistance in cell sorting and image quantification, and S. Soto and H. Popper for pathology analysis of tumor metastases. We thank A. L. Prieto, E. Vivier, D. Raulet, and C. Melief for providing us with critical reagents and C. Martinez, A. Majoros and P.C. Esk for sharing reagents and helpful discussions. We also thank G. Kéri, L. Örfi and colleagues from Vichem Kft., Budapest, Hungary for their initial synthetic work on the quinoline-based Axl inhibitors, which served as the basis for the current rationale design of LDC1267. M.P. is supported by the ERC and Era of Hope/DoD Innovator Award. J.M.P. is supported by grants from IMBA, the Austrian National Foundation, the Austrian Academy of Sciences, GEN-AU (AustroMouse), and Era of Hope/DoD Innovator Award, and an EU ERC Advanced Grant.

References

1. Brabletz T, Lyden D, Steeg PS, Werb Z. Roadblocks to translational advances on metastasis research. Nature Med. 2013; 19:1104–1109. [PubMed: 24013756]

2. Pardoll DM. The blockade of immune checkpoints in cancer immunotherapy. Nature Rev Cancer. 2012; 12:252–264. [PubMed: 22437870]
3. Lacour F, Oberling C, Guerin M. Effect of dicoumarol on the development of metastases of the T8 epithelioma in the rat; new research. Bull Assoc Fr Etud Cancer. 1957; 44:88–91. [PubMed: 13460416]
4. Loeser S, et al. Spontaneous tumor rejection by cbl-b-deficient $CD8^+$ T cells. J Exp Med. 2007; 204:879–891. [PubMed: 17403934]
5. Chiang JY, Jang IK, Hodes R, Gu H. Ablation of Cbl-b provides protection against transplanted and spontaneous tumors. J Clin Invest. 2007; 117:1029–1036. [PubMed: 17364027]
6. Paolino M, et al. Essential role of E3 ubiquitin ligase activity in Cbl-b-regulated T cell functions. J Immunol. 2011; 186:2138–2147. [PubMed: 21248250]
7. Oksvold MP, Dagger SA, Thien CB, Langdon WY. The Cbl-b RING finger domain has a limited role in regulating inflammatory cytokine production by IgE-activated mast cells. Mol Immunol. 2008; 45:925–936. [PubMed: 17868870]
8. Kojo S, et al. Mechanisms of NKT cell anergy induction involve Cbl-b-promoted monoubiquitination of CARMA1. Proc Natl Acad Sci. 2009; 106:17847–17851. [PubMed: 19815501]
9. Makino Y, Kanno R, Ito T, Higashino K, Taniguchi M. Predominant expression of invariant V alpha 14+ TCR alpha chain in NK1.1+ T cell populations. Intern Immunol. 1995; 7:1157–1161.
10. Pannellini T, Forni G, Musiani P. Immunobiology of her-2/neu transgenic mice. Breast Dis. 2004; 20:33–42. [PubMed: 15687705]
11. Linger RM, Keating AK, Earp HS, Graham DK. TAM receptor tyrosine kinases: biologic functions, signaling, and potential therapeutic targeting in human cancer. Adv Cancer Res. 2008; 100:35–83. [PubMed: 18620092]
12. Nagata K, et al. Identification of the product of growth arrest-specific gene 6 as a common ligand for Axl, Sky, and Mer receptor tyrosine kinases. J Biol Chem. 1996; 271:30022–30027. [PubMed: 8939948]
13. Caraux A, et al. Natural killer cell differentiation driven by Tyro3 receptor tyrosine kinases. Nat Immunol. 2006; 7:747–754. [PubMed: 16751775]
14. Lemke G, Rothlin CV. Immunobiology of the TAM receptors. Nature Rev Immunol. 2008; 8:327–336. [PubMed: 18421305]
15. Pulaski BA, Ostrand-Rosenberg S. Mouse 4T1 breast tumor model. Curr Protoc Immunol. 2001 Chapter 20, Unit 20 22.
16. Pirmohamed M. Warfarin: almost 60 years old and still causing problems. Br J Clin Pharmacol. 2006; 62:509–511. [PubMed: 17061959]
17. Ryan JJ, Ketcham AS, Wexler H. Reduced incidence of spontaneous metastases with long-term Coumadin therapy. Ann Surg. 1968; 168:163–168. [PubMed: 5673195]
18. McCulloch P, George WD. Warfarin inhibits metastasis of Mtln3 rat mammary carcinoma without affecting primary tumour growth. Br J Cancer. 1989; 59:179–183. [PubMed: 2930682]
19. Brown JM. A study of the mechanism by which anticoagulation with warfarin inhibits blood-borne metastases. Cancer Res. 1973; 33:1217–1224. [PubMed: 4718672]
20. Hasanbasic I, Rajotte I, Blostein M. The role of gamma-carboxylation in the anti-apoptotic function of gas6. J Thromb Haemost. 2005; 3:2790–2797. [PubMed: 16359517]
21. Yanagita M, et al. Gas6 regulates mesangial cell proliferation through Axl in experimental glomerulonephritis. Am J Pathol. 2001; 158:1423–1432. [PubMed: 11290560]
22. Nagai K, et al. Growth arrest-specific gene 6 is involved in glomerular hypertrophy in the early stage of diabetic nephropathy. J Biol Chem. 2003; 278:18229–18234. [PubMed: 12644472]
23. Lu Q, Lemke G. Homeostatic regulation of the immune system by receptor tyrosine kinases of the Tyro 3 family. Science. 2001; 293:306–311. [PubMed: 11452127]
24. Haglund K, Dikic I. The role of ubiquitylation in receptor endocytosis and endosomal sorting. J Cell Sci. 2012; 125:265–275. [PubMed: 22357968]
25. Valverde P. Effects of Gas6 and hydrogen peroxide in Axl ubiquitination and downregulation. Biochem Biophys Res Commun. 2005; 333:180–185. [PubMed: 15958209]

26. Caspi RR. Immunotherapy of autoimmunity and cancer: the penalty for success. Nature Rev Immunol. 2008; 8:970–976. [PubMed: 19008897]
27. Bachmaier K, et al. Negative regulation of lymphocyte activation and autoimmunity by the molecular adaptor Cbl-b. Nature. 2000; 403:211–216. [PubMed: 10646608]
28. Lee-MacAry AE, et al. Development of a novel flow cytometric cell-mediated cytotoxicity assay using the fluorophores PKH-26 and TO-PRO-3 iodide. J Immunol Methods. 2001; 252:83–92. [PubMed: 11334968]
29. Cerwenka A, Baron JL, Lanier LL. Ectopic expression of retinoic acid early inducible-1 gene (RAE-1) permits natural killer cell-mediated rejection of a MHC class I-bearing tumor in vivo. Proc Natl Acad Sci. 2001; 98:11521–11526. [PubMed: 11562472]
30. Harshan KV, Gangadharam PR. In vivo depletion of natural killer cell activity leads to enhanced multiplication of Mycobacterium avium complex in mice. Infect Immun. 1991; 59:2818–2821. [PubMed: 1855997]
31. Jamieson AM, et al. The role of the NKG2D immunoreceptor in immune cell activation and natural killing. Immunity. 2002; 17:19–29. [PubMed: 12150888]
32. Carlyle JR, et al. Molecular and genetic basis for strain-dependent NK1.1 alloreactivity of mouse NK cells. J Immunol. 2006; 176:7511–7524. [PubMed: 16751398]
33. Kasai M, et al. In vivo effect of anti-asialo GM1 antibody on natural killer activity. Nature. 1981; 291:334–335. [PubMed: 7231554]
34. Walzer T, et al. Identification, activation, and selective in vivo ablation of mouse NK cells via NKp46. Proc Natl Acad Sci. 2007; 104:3384–3389. [PubMed: 17360655]
35. Roepstorff K, et al. Differential effects of EGFR ligands on endocytic sorting of the receptor. Traffic. 2009; 10:1115–1127. [PubMed: 19531065]
36. Schultz-Fademrecht C, , et al. Pharmaceutically active compounds as Axl inhibitors. Patent application. EP2423208 A1. 2012.
37. Godl K, et al. An efficient proteomics method to identify the cellular targets of protein kinase inhibitors. Proc Natl Acad Sci. 2003; 100:15434–15439. [PubMed: 14668439]
38. Brehmer D, Godl K, Zech B, Wissing J, Daub H. Proteome-wide identification of cellular targets affected by bisindolylmaleimide-type protein kinase C inhibitors. Mol Cell Proteomics. 2004; 3:490–500. [PubMed: 14769951]

Europe PMC Funders Author Manuscripts

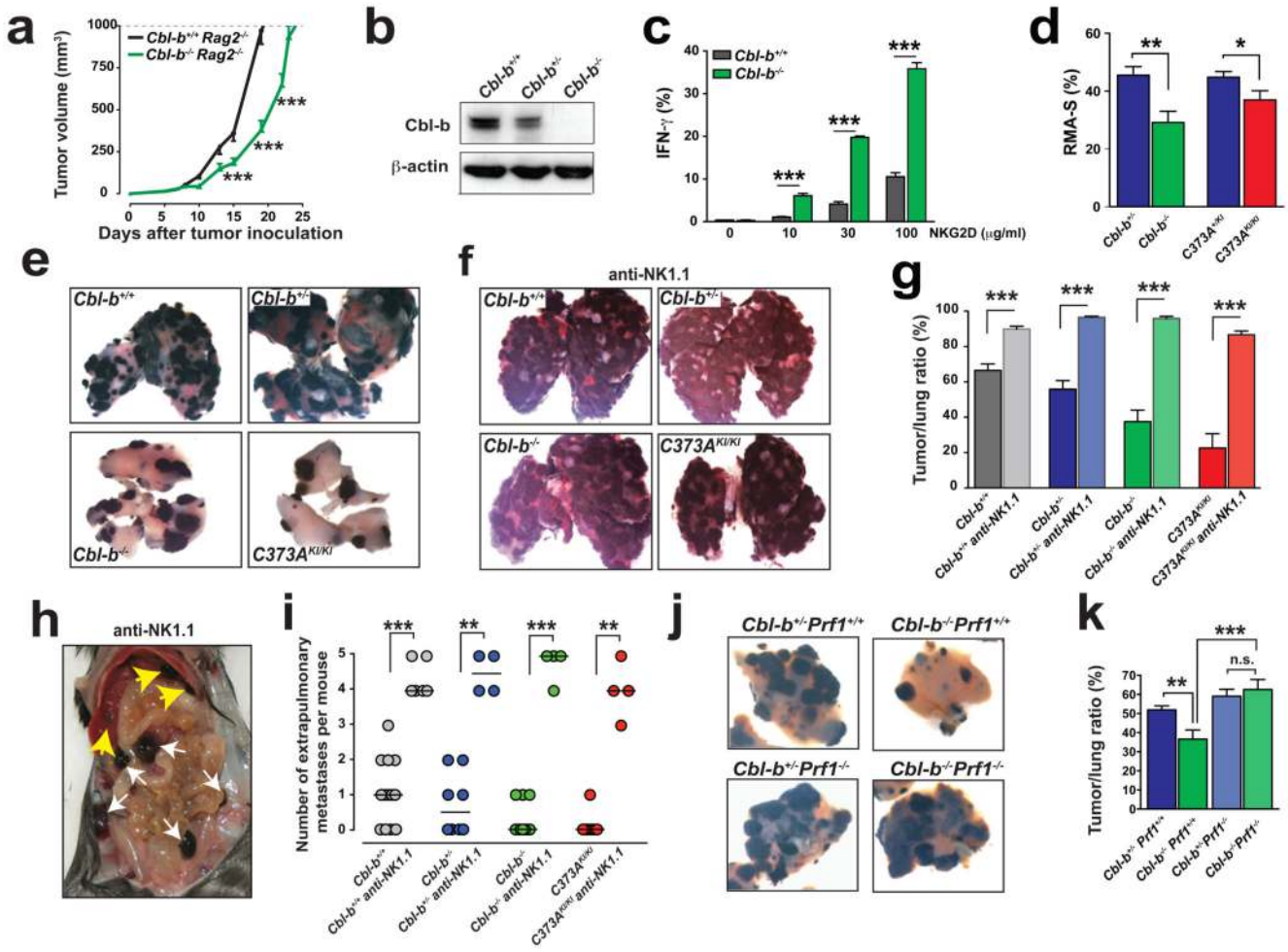

Figure 1. *Cbl-b* mutant NK cells control metastatic melanomas.

a, TC-1 tumor growth in *Cbl-b*$^{+/+}$*Rag2*$^{-/-}$ and *Cbl-b*$^{-/-}$*Rag2*$^{-/-}$ mice (mean ± s.e.m., n=10 each). ***P<0.001 (two-way ANOVA, Bonferroni's post hoc test). **b,** Cbl-b and β-actin protein expression in *Cbl-b*$^{+/+}$, *Cbl-b*$^{+/-}$, and *Cbl-b*$^{-/-}$ NK cells. **c,** IFN-γ^{+} *Cbl-b*$^{+/+}$ and *Cbl-b*$^{-/-}$ NK cells (%) following anti-NKG2D stimulation. (mean ± s.e.m., n=3).***P<0.001 (two-way ANOVA, Bonferroni's post hoc test). **d,** *In vivo* NK cell cytotoxicity towards RMA-S cells (mean ± s.e.m., n=16/10/15/14). *P<0.05, **P<0.01 (Student's t-test). **e, f,** Representative lung melanoma metastases in control (**e**) or NK.1.1-depleted *Cbl-b*$^{+/+}$, *Cbl-b*$^{+/-}$, *Cbl-b*$^{-/-}$, and *C373A*$^{KI/KI}$ mice (**f**) at day+21. **g,** B16F10 tumor-to-lung ratios (mean ± s.e.m.) of control and NK1.1^{+}-depleted *Cbl-b*$^{+/+}$(n=12/6), *Cbl-b*$^{+/-}$ (n=6/4), *Cbl-b*$^{-/-}$ (n=9/4), and *C373A*$^{KI/KI}$ (n=7/4) mice. ***P<0.001 (Student's t-test). **h,** Representative B16F10 extrapulmonary metastases in a NK1.1^{+} cell depleted mouse. **i,** Extrapulmonary metastases in control or NK1.1-depleted mice (lines are median, day+16-21) **P<0.01***P<0.001 (Mann-Whitney test). **j, k,** Representative B16F10 lung metastases **(j)** and tumor-to-lung ratios **(k)** (mean ± s.e.m., day+21) in *Cbl-b*$^{+/-}$ *Prf1*$^{+/+}$, *Cbl-b*$^{-/-}$ *Prf1*$^{+/+}$, *Cbl-b*$^{+/-}$ *Prf1*$^{-/-}$ and *Cbl-b*$^{-/-}$ *Prf1*$^{-/-}$ mice. n=5/7/8/8. **P<0.01, ***P<0.001, n.s., not significant (One-way ANOVA, Tukey's post hoc test).

Europe PMC Funders Author Manuscripts

Europe PMC Funders Author Manuscripts

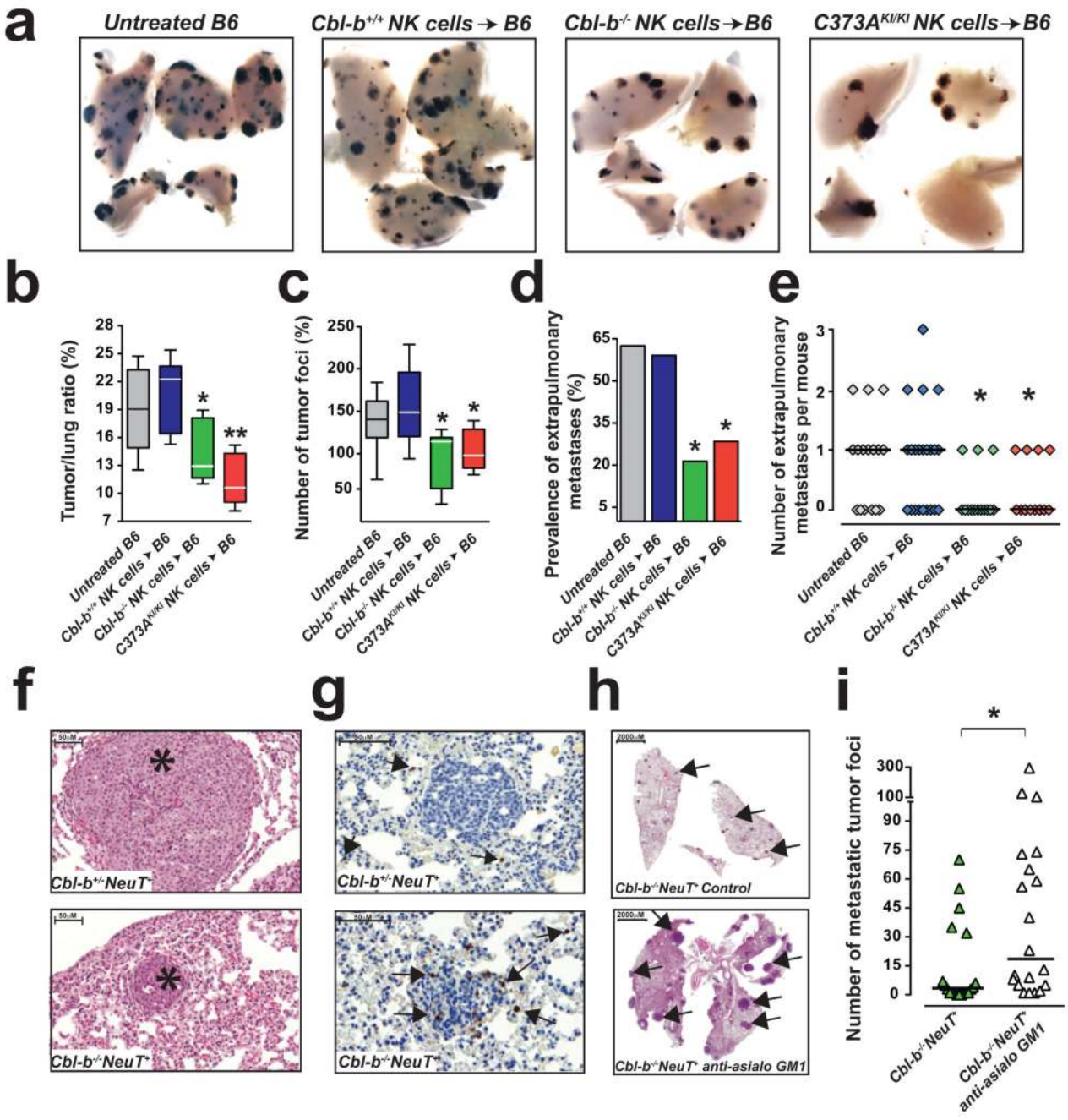

Figure 2. Therapeutic anti-tumor activity of *Cbl-b* mutant NK cells.

a-d, Representative lung metastases (**a**), tumor-to-lung ratios (**b**), numbers of tumor foci (**c**), prevalence (**d**) and numbers of extrapulmonary metastases (**e**) at day+14 in C57BL/6J mice untreated or adoptively transferred with *Cbl-b*$^{+/+}$, *Cbl-b*$^{-/-}$, and *C373A*$^{KI/KI}$ NK cells. For **b** and **c**, n=6/6/6/7, *P<0.05 and **P<0.001 (Mann-Whitney test). For **d** and **e**, n=16/22/14/15, *P<0.05 (Chi-square test in **d** and Mann-Whitney test in **e**). **f, g,** Metastases (**f,** H&E, asterix) and NKp46^{+} NK cells (**g**, arrows) in lungs of *Cbl-b*$^{+/-}$*NeuT*$^{+}$ and *Cbl-b*$^{-/-}$*NeuT*$^{+}$ mice. n=17/20. **h,i,** Representative H&E-stained lung metastases (**h,** arrows) and number of

metastatic foci (**i**) in control and anti-asialo GM1-treated *Cbl-b*$^{-/-}$*NeuT*$^{+}$ mice. n=11/10. *P<0.05 (Mann-Whitney test, lines are median). Bars, 50μM (**f** and **g**), 2000 μM (**h**)

Europe PMC Funders Author Manuscripts

Europe PMC Funders Author Manuscripts

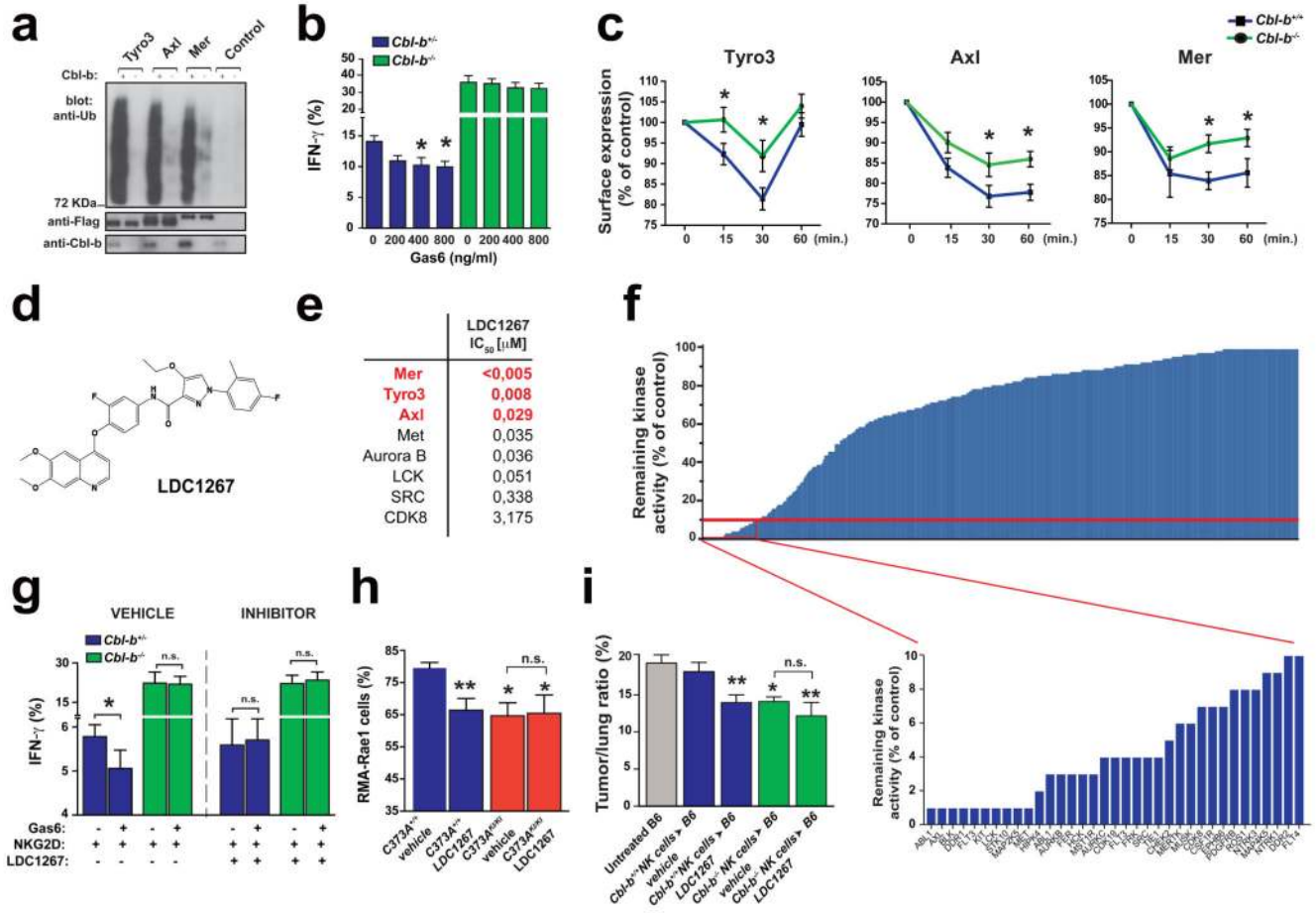

Figure 3. TAM receptors are Cbl-b targets and characterization of a TAM receptor blocker.

a, *In vitro* Cbl-b-dependent ubiquitylation of Tyro3, Axl, and Mer (anti-Ub). Control, no TAM receptors. Loading controls are shown. **b,** IFN-γ$^+$ *Cbl-b*$^{+/+}$ and *Cbl-b*$^{-/-}$ NK cells (%) stimulated with anti-NKG2D Abs in the presence of soluble Gas6. *P<0.05 (One-way ANOVA, Dunnett's post hoc test, n=6/5). **c,** TAM receptors surface expression in NK cells after stimulation with Gas6. *P<0.05 (two-way ANOVA, Bonferroni's post hoc test, n=10-13). **d,** Chemical structure of the TAM receptor kinase inhibitor LDC1267. **e,** IC_{50} values for the indicated protein kinases as determined by tracer assays. **f,** Remaining activity (compared to DMSO control) in 456 kinases treated with 1μM LDC1267 **g,** IFN-γ$^+$ *Cbl-b*$^{+/+}$ and *Cbl-b*$^{-/-}$ NK cells (%) pre-treated with vehicle or LDC1267 and then stimulated with anti-NKG2D Abs and Gas6. *P<0.05, n.s., not significant (Student's t-test, n=11/8.). **h,** *In vivo* NK cytotoxicity towards RMA-Rae1 cells in mice treated with vehicle or LDC1267. *P<0.05, **P<0.01 (One-way ANOVA, Tukey's post hoc test, n=16/14/9/10). **i,** Tumor-to-lung areas in B16F10 tumor-bearing B6 mice untreated or adoptively transplanted with NK cells *ex vivo* treated with vehicle or LDC1267. *P<0.05 and **P<0.01 (One-way ANOVA, Tukey's post hoc test, n=16/16/16/10/10). Data in **b**,**c**,**g-i** are mean ± s.e.m.

Europe PMC Funders Author Manuscripts

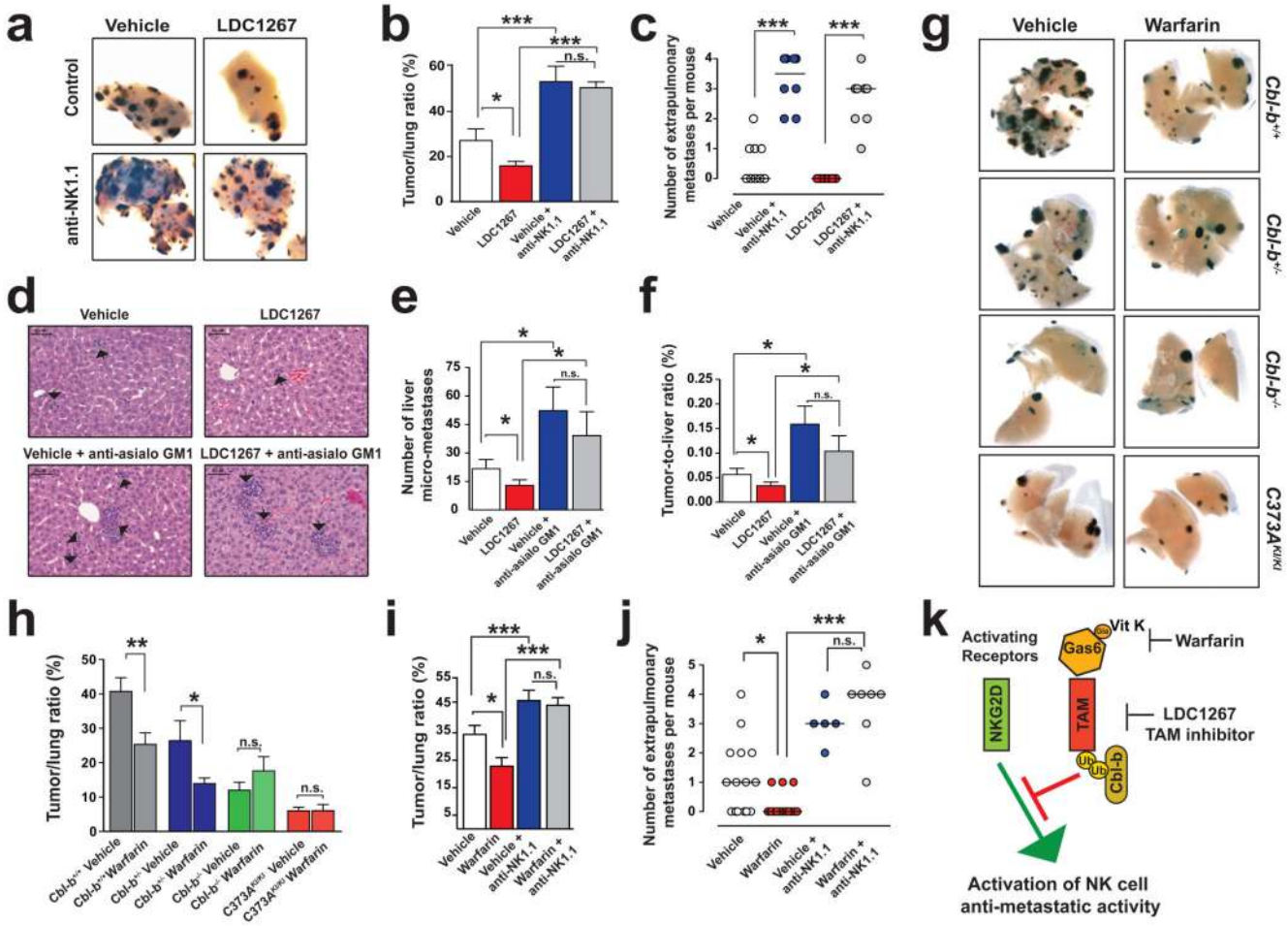

Figure 4. Control of metastases by TAM receptor inhibition.

a-c, Lung melanoma metastases (**a**), tumor-to-lung ratios (**b**, mean ± s.e.m.), and extrapulmonary metastases (**c**, lines are median) in vehicle- and LDC1267-treated wild-type control or NK1.1-depleted mice. n=8 each. *P<0.05, ***P<0.001, n.s., not significant (Student's t-test in **b** and Mann-Whitney test in **c**). **d-f,** Representative images (**d**, arrows; bars, 50μm), and numbers (**e**) and relative sizes (**f**) of 4T1 liver micro-metastasis in control or asialo-GM1 immunodepleted mice treated with vehicle or LDC1267 (20mg/kg, daily i.p.). Mean ± s.e.m., n=7/9/8/8. *P<0.05; n.s., not significant (Mann-Whitney test). **g,h,** Representative lung B16F10 melanoma metastases (**g**) and tumor-to-lung ratios (**h**) in vehicle and warfarin-treated (0.5 mg/l) *Cbl-b*$^{+/+}$ (n=12/12), *Cbl-b*$^{+/-}$ (n=6/7), *Cbl-b*$^{-/-}$ (n=4/7), and *C373A*$^{KI/KI}$ (n=8/8) mice. Mean ± s.e.m.**P<0.01, *P<0.05, n.s., not significant (Student's t-test). **i, j,** Relative lung tumor area (**i**, mean ± s.e.m.) and extrapulmonary melanoma metastases (**j**, lines are median) in *Cbl-b*$^{+/+}$ mice treated with vehicle (n=15), warfarin (n=14), vehicle and anti-NK1.1 Abs (n=5) or warfarin and anti-NK1.1 Abs (n=7). *P<0.05, ***P<0.001, n.s., not significant (One-way ANOVA, Tukey's post hoc test for **i**; Mann-Whitney test for **j**). **k,** Schematic illustrating the TAM receptor/Cbl-b inhibitory pathway controlling NK cell anti-metastatic activities.